11-day-old Wistar rats (Hartey, SLC, Japan) were killed by decapitation according to the guidelines for animal experimentation at Kobe University School of Medicine. The hippocampus was rapidly dissected at 4–6 °C and cut into 400-μm slices using a Mcillwain Tissue Chopper (Mickle Laboratory Engineering Co. Ltd, UK). The slices were immediately placed onto a 30-μm-diameter pored membrane (Millicell-CM, Millipore, Bedford MA, USA), transferred into a six-well microplate (Costar Corning Inc., NY, USA, four slices per well) with 1 mL slice culture medium per well and finally maintained at 37 °C in a 95% humidified atmosphere with 5% CO_2 incubator (Sanyo, Tokyo, Japan). The slice culture medium consisted of 50% minimum essential medium (MEM; Gibco, CA, USA), 25% Hanks' balanced salt solution (HBSS; Gibco), 25% heat inactivated horse serum (Gibco) supplemented 6.5 mg/mL glucose, 1% penicillin/streptomycin, and 1% Glutamax-‡T (Gibco). The medium was changed every 3 days and cultures were used for the experiments after 14 days in vitro.

Treatment of hippocampal slices

After 14 days in vitro, the slices were washed, and then exposed for 24 or 48 h to glucose (10 mM), pyruvate (10 mM), lactate (10 mM), sucrose (10 mM) medium, or to the combinations of glucose (10 mM) with pyruvate (5 mM), pyruvate (10 mM), lactate (5 mM), trolox (1 mM), niacinamide (10 mM) or α-cyano-4-hydroxycinnamic acid (4-CIN; 0.2 mM). All the reagents listed above were supplemented in a serum-free and glucose-free medium containing 90 mM NaCl, 4 mM KCl, 0.1 mM KHPO$_4$, 0.1 mM $MgCl_2$, 0.5 mM $MgSO_4$, 0.1 mM Na_2HPO_4, 0.5 mM NaH_2PO_4, 14 mM $NaHCO_3$, 1.2 mM $CaCl_2$, 2 mM essential and non-essential amino acids, 0.02 mM vitamins, 1% Glutamax-‡T, and 2% B-27 supplement without antioxidants (Gibco), without or with 40 μM Aβ$_{25-35}$.

To establish the Aβ-induced neurotoxicity, slices were treated with two kinds of Aβ peptides (Aβ$_{25-35}$ and Aβ$_{1-42}$; Peptide Institute Inc., Osaka, Japan) in various concentrations. To obtain the oligomer of Aβ, Aβ was pretreated before applying it to each medium according to Roselli's method (Roselli et al., 2005). Aβ was dissolved in DMSO at 2 mM, and thereafter it was diluted ten-fold in sterile PBS, vortexed for 30 min (at room temperature), and centrifuged at 15 000g at 4 °C for 1 h. The supernatant (180 μM) was aliquoted (100 μL) and frozen at −20 °C. Aliquots were diluted in culture medium to a final concentration immediately before use.

Assessment of cell death in hippocampal slices

The propidium iodide (PI) method was applied for the assessment of neuron death in hippocampal slices at 6, 24 and 48 h after each treatment in the CA1 region of the hippocampus. To label the nuclei of dead neurons, 4.6 μg/mL PI (Sigma, Louis St, MO, USA) was added to the wells of the culture microplates for 20 min. PI is a polar compound which only enters cells with damaged cell membranes. Inside the cells it binds to nucleic acids and becomes brightly red fluorescent. The dye is basically non-toxic to neurons and has been used as an indicator of neuronal integrity and cell viability (Macklis & Madison, 1990). Thus, the intensity of fluorescence is parallel to the cell death. After 20 min, digital imagines of PI fluorescence were obtained with an inverted fluorescence microscope (4× objective) equipped with a digital camera (Olympus IX70, Tokyo, Japan). After 14 days of in vitro culture, prior to conditioning the slices, the PI fluorescence intensity was adjusted to zero equivalent to the negative control (0% cell

death). After the final image, all the living neurons were killed by adding 10 μM N-methyl-D-aspartic acid (NMDA; Sigma) and the final PI fluorescence intensity was adjusted to 100% equivalent to total neuronal cell death. The mean intensity (green values) of the PI fluorescence was measured using an image program Lumina Vision (v.24.3; Mitani Inc., Osaka, Japan).

Determination of aconitase activity

Aconitase activity was measured at 24 h after each treatment. Four slices were immediately homogenized in homogenization buffer, which consists of 50 mM Tris-HCl$_2$, pH 7.6, containing 1 mM cysteine, 1 mM citrate and 0.5 mM $MnCl_2$, and aconitase activity was then measured immediately to avoid any inactivation by O_2 after the extract had been centrifuged. Aconitase activity was measured in an assay medium containing the following: 50 mM Tris-HCl$_2$, 0.6 mM $MnCl_2$, 6 mM sodium citrate, 0.2% Triton X-100, 2 U/mL isocitrate dehydrogenase (NADP$^+$-dependent), and 1 U/mL catalase at 37 °C, pH 7.4. The reaction was initiated by the addition of 0.2 mM NADP$^+$. The fluorescence intensity was determined with a Wallac 1420 ARVOsx (Perkin Elmer Life Science, Tokyo, Japan) at 340 nm (Tretter et al., 2005).

Measurement of ATP levels

At 6 or 24 h after each treatment, four slices were immediately homogenized in 0.5 mM perchloric acid with 1 mM thylene-diamine-tetra acetic acid and centrifudged for 15 min at 300 g. The supernatant was neutralized with 2 M K_2HCO_4, recentrifuged and stored at −30 °C until assay of ATP. ATP was quantified by a luciferin-luciferase luminescence assay (Sigma). The protein content of the slices was determined by the method of Lowry and Passonneau (Okada, 1974).

Determination of NAD$^+$ levels

The NAD$^+$ levels of hippocampal slices were measured at 6 or 24 h after each treatment. Four slices were immediately homogenized by addition of 75% ethanol–0.05 M K_2HPO_4. Protein was precipitated by the addition of 0.02 M ZnCl and centrifuged at 13 000g at 4 °C for 15 min; the supernatant was stored at −80 °C until assay of NAD$^+$ levels (Tilton et al., 1991). NAD$^+$ was measured after its enzymatic conversion to NADH by alcohol dehydrogenase, thus resulting in an increase in the fluorescence spectrum between 400 and 600 nm after an excitation at 340 nm using a Wallac 1420 ARVOsx (Perkin Elmer life science, Tokyo, Japan) (Sander et al., 1976).

Materials

Trolox was purchased from Calbiochem (Darmstadt, Germany). Sodium pyruvate, sodium lactate, and 4-CIN were obtained from Sigma, and all other chemicals were from Wako (Tokyo, Japan) or Nacalai (Kyoto, Japan).

Statistical analysis

The data were expressed as the mean ± standard error of the mean (SEM) from three independent experiments. Statistical significance was established by ANOVA followed by Fisher's PLSD post-hoc test using Statview (v.5.0.1.0; SAS Institute Inc., Cary, NC, USA)

software. A value of $P < 0.05$ was considered to be statistically significant.

Results

$A\beta_{1-42}$ and $A\beta_{25-35}$ show similar toxic effects

Two different Aβ fragment types, $A\beta_{25-35}$ and $A\beta_{1-42}$, were applied to establish the neurotoxicity of Aβ. Cell death was evaluated at 48 h after administration of various concentrations of the two Aβ fragments. $A\beta_{1-42}$ caused 4.2–18% cell death at concentrations ranging from 0.5 to 25 μM. $A\beta_{25-35}$ (40 μM) induced toxicity comparable with that for $A\beta_{1-42}$ at 15 μM (data not shown). As $A\beta_{25-35}$ and full-length $A\beta_{1-42}$ cause neuron death by similar mechanisms (Mattson *et al.*, 1997), $A\beta_{25-35}$ at 40 μM was used in all subsequent experiments.

Glucose demonstrated a better neuroprotective effect on neuronal survival than MCTs alone in the absence and presence of Aβ

To examine whether the replacement of glucose with MCTs (particularly lactate and pyruvate) had an equivalent effect as glucose on neuronal survival in the hippocampal slice cultures and ameliorate the neurotoxicity induced by Aβ, cell death was assessed by a PI assay at 24 and 48 h after each replacement. In comparison with glucose, which induced 2.2 ± 1.2% cell death, both pyruvate and lactate alone increased cell death in the hippocampal slice cultures at 24 h (3.1 ± 0.5 and 3.3 ± 0.7% cell death, respectively, $P < 0.05$) and 48 h (5.5 ± 0.6 and 5.8 ± 0.5% cell death, respectively, $P < 0.05$), and sucrose significantly increased cell death more than pyruvate and lactate (6.2 ± 0.5 and 9.0 ± 1.3% cell death, $P < 0.001$) (Fig. 1A), indicating that pyruvate and lactate alone were not as effective as glucose, but were much better than sucrose. Similar results were obtained in the hippocampal slice cultures treated with 40 μM $A\beta_{25-35}$ (Fig. 1B). Pyruvate, lactate or sucrose alone facilitated cell death in the presence of 40 μM $A\beta_{25-35}$ for 24 h (Figs 1B and 3B–D). When pyruvate was added with glucose, Aβ toxicity was significantly ameliorated, as shown by the decrease of PI fluorescence intensity (Fig. 3E). These results demonstrate that pyruvate and lactate alone cannot be replaced for glucose to preserve the neuronal viability in the hippocampal slice cultures, and they alone cannot ameliorate Aβ neurotoxicity.

Pyruvate supplementation ameliorates the neurotoxicity in the glucose-containing medium and also protects against Aβ neurotoxicity

We next assumed that monocarboxylate might work for neuronal survival as a fundamental energy source if glucose was present in the culture medium. We treated the hippocampal slice cultures with a glucose-containing medium supplemented with pyruvate, lactate, niacinamide, trolox or 4-CIN for 24 h (Fig. 2A). The results showed that glucose + pyruvate (10 mM) decreased cell death by 54.6 ± 1.2% ($P < 0.01$), but that glucose + lactate did not have a similar protective effect. The free radical scavenger trolox and the NAD^+ precursor niacinamide can also decrease cell death after being added to a glucose-containing medium by 27.3 ± 0.6% ($P < 0.05$) and 31.8 ± 0.6% ($P < 0.05$), respectively. The pyruvate additive effect was reversed in the presence of 4-CIN, a specific inhibitor of the monocarboxylate transporter. Moreover, the presence of 4-CIN
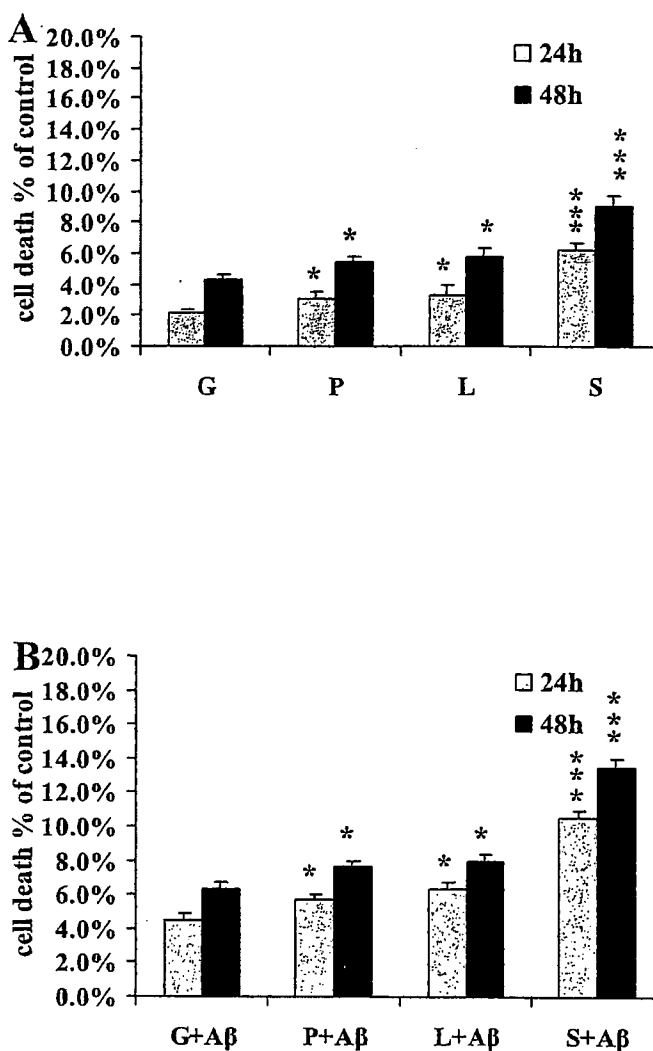

FIG. 1. Effects of the individual treatment of glucose (G: 10 mM), pyruvate (P: 10 mM), lactate (L: 10 mM), sucrose (S: 10 mM) on cell death in hippocampal organotypic slices culture (A) and on cell death induced by $A\beta_{25-35}$ (40 μM) (B). After 24 and 48 h, neuronal death was evaluated by propidium iodide staining. Vertical bars indicate SEM, $n = 12$. Asterisks show significant differences between the glucose treatment and other conditions at $*P < 0.05$, $***P < 0.001$ by ANOVA [A: $F_{3,44} = 128.761$ (24 h), $F_{3,44} = 71.867$ (48 h); B: $F_{3,44} = 131.596$ (24 h), $F_{3,44} = 142.963$ (48 h)] followed by Fisher's PLSD *post-hoc* test. No significant difference was observed between the pyruvate and lactate conditions either without or with Aβ ($P > 0.05$) (A and B).

increased the cell death by 186.4 ± 4.1% ($P < 0.001$) of the control condition in the presence of glucose, thus indicating cell toxicity even at low concentration, 200 μM (Fig. 2A). Aβ-induced neurotoxicity in the hippocampal slice cultures was ameliorated by pyruvate (decreased cell death by 56 ± 2.8%, $P < 0.01$) (Fig. 3E), trolox (decreased cell death by 34 ± 1.7%, $P < 0.05$) and niacinamide (decreased cell death by 40 ± 1.9%, $P < 0.05$) in the presence of glucose. The protective effects of these applications were also abolished by 4-CIN (increased cell death by 58 ± 2.9%, $P < 0.01$) (Fig. 2B). These results suggest that, in a glucose-containing medium, pyruvate improves neuronal survival in the hippocampal slice cultures and also protects neurons against Aβ-induced cell death, and its protective effect is as strong as those of trolox, an ROS scavenger, and niacinamide, an NAD^+ precursor.

A
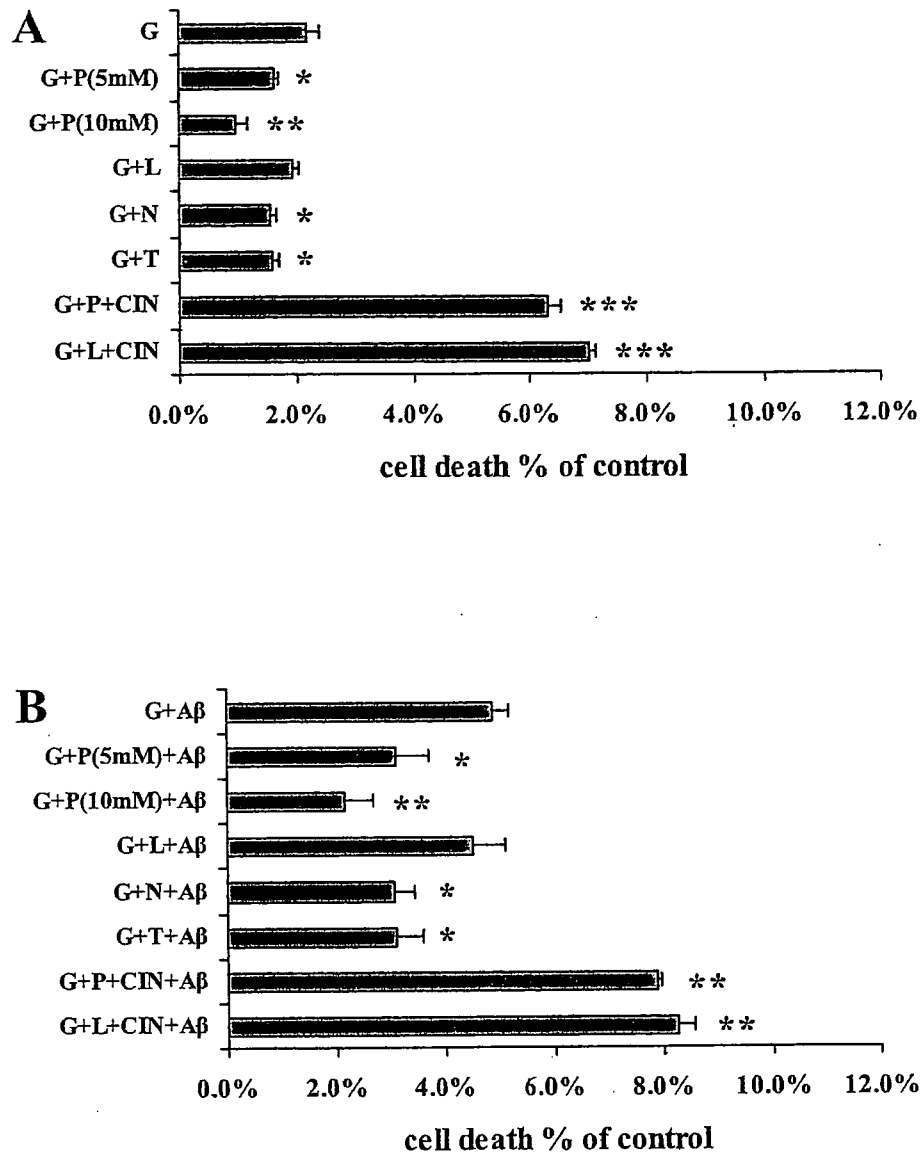
- G
- G+P(5mM) *
- G+P(10mM) **
- G+L
- G+N *
- G+T *
- G+P+CIN ***
- G+L+CIN ***

0.0% 2.0% 4.0% 6.0% 8.0% 10.0% 12.0%

cell death % of control

B

- G+Aβ
- G+P(5mM)+Aβ *
- G+P(10mM)+Aβ **
- G+L+Aβ
- G+N+Aβ *
- G+T+Aβ *
- G+P+CIN+Aβ **
- G+L+CIN+Aβ **

0.0% 2.0% 4.0% 6.0% 8.0% 10.0% 12.0%

cell death % of control

FIG. 2. Effects of the supplementation of glucose-containing culture media with pyruvate (P: 5 mM and 10 mM), lactate (L: 5 mM), trolox (T: 1 mM), niacinamide (N: 10 mM) and 4-CIN (0.2 mM) on cell death in hippocampal organotypic slice cultures in the absence (A) and presence (B) of $A\beta_{25-35}$ (40 μM) after 24 h. In comparison to G, G + P (5 mM), G + P (10 mM), G + T and G + N significantly reduced cell death, but G + L did not. The presence of 4-CIN reversed the protective effect of pyruvate and showed an increased level of cell death as compared with glucose treatment. In the presence of Aβ, pyruvate, nictinamide and trolox showed a significant protective effect against Aβ toxicity, but this was not the case for addition of lactate. Horizontal bars indicate SEM, $n = 12$. Asterisks show significant differences between the glucose treatment and other conditions at $*P < 0.05$, $**P < 0.01$, $***P < 0.001$ by ANOVA (A: $F_{7,88} = 46.739$; B: $F_{7,88} = 33.917$) followed by Fisher's PLSD post-hoc test.

To determine whether the protective effect of pyruvate on neuronal cell death could be extended to physiologically relevant peptides, the hippocampal slice cultures were exposed to 20 μM $A\beta_{1-42}$, and cell death was examined after 24 and 48 h of treatment. The addition of pyruvate in the glucose-containing medium also decreased the cell death induced by 20 μM $A\beta_{1-42}$ by 58.2 ± 7.8% ($P < 0.01$, 24 h) and 53.5 ± 6.2% ($P < 0.01$, 48 h).

Protective effect of pyruvate on aconitase activity of hippocampal slices in the presence of Aβ

It has been demonstrated previously that detection of aconitase activity can be used as an indicator of ROS production (Liang et al., 2000;

Tretter et al., 2000). ROS generation by in situ mitochondria in synaptosomes paralleled a decrease in the activity of aconitase (Sipos et al., 2003). Therefore, it was expected in the present study that when hippocampal slices were incubated with Aβ that would induce ROS production, the activity of aconitase would decrease. When the hippocampal slices were incubated with 40 μM $A\beta_{25-35}$, aconitase activity decreased to 58.1% of the control in the medium including glucose. In the presence of glucose, the addition of pyruvate and trolox increased aconitase activity up to 85.5 and 84.2%, respectively, but the addition of lactate and niacinamide demonstrated no improvements in aconitase activity (56.5 and 60.3%, respectively) (Fig. 4). These results indicate that pyruvate, but not lactate, has a protective effect as strong as trolox, a well-known ROS scavenger.
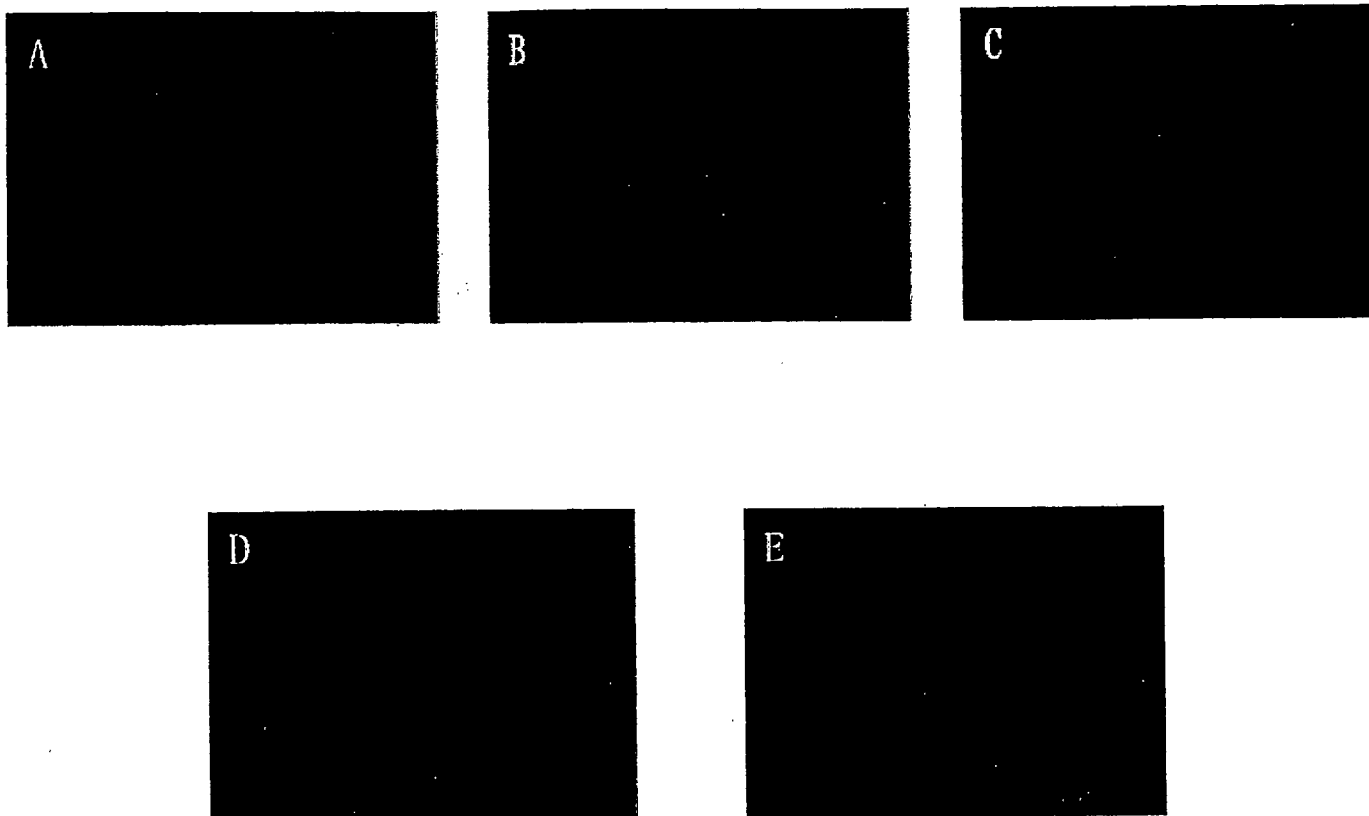
FIG. 3. Cell death induced by $A\beta_{25-35}$ in hippocampal organotypic slice cultures and the neuroprotective effects of pyruvate in the presence of glucose. Fluorescence images of organotypic hippocampal slice cultures exposed to $A\beta_{25-35}$ treated with glucose 10 mM (A), pyruvate 10 mM (B), lactate 10 mM (C), sucrose 10 mM (D), and glucose 10 mM plus pyruvate 10 mM (E).

Effect of MCTs on the ATP levels of hippocampal slices in the presence of Aβ

To test the hypothesis that the neuroprotective effect of pyruvate against Aβ-induced neurotoxicity was due to its role as an alternative energy source, we examined the effect of MCT on the ATP levels in hippocampal slices in the presence of Aβ. ATP levels in the slices at 24 h are 10.2 ± 0.94 mmol/kg protein under the control condition (10 mM glucose, in the absence of Aβ). In comparison with the control group, incubation with 40 μM $A\beta_{25-35}$ caused a significant decrease of ATP levels in both the glucose (68.6% of the control) and MCT groups (69.0% of the control in 5 mM pyruvate and 68.8% of the control in 5 mM lactate) ($P < 0.05$). In comparison with glucose, neither glucose + pyruvate nor glucose + lactate ameliorated the decrease of ATP levels in the presence of Aβ (Fig. 5). These results suggest that the protective effect of pyruvate on neuronal survival cannot be explained by its role as an energy substrate. In addition, pyruvate cannot preserve the ATP levels of the slice, while it leads to significant cell protection against Aβ (Figs 2B and 3E).

Effect of MCTs on NAD+ levels of hippocampal slices in the presence of Aβ and correlation between neuronal cell death and NAD+ levels in hippocammpal organotypic slice cultures

The mitochondrial NAD(P) redox status has been demonstrated to play a central role in the neuroprotective properties of the pyruvate supply (Alvarez *et al.*, 2003), and NAD^+ treatment attenuated Aβ generation in the primary Tg2576 neuron cultures (Qin *et al.*, 2006). We herein examined the effect of MCTs on the NAD^+ levels in
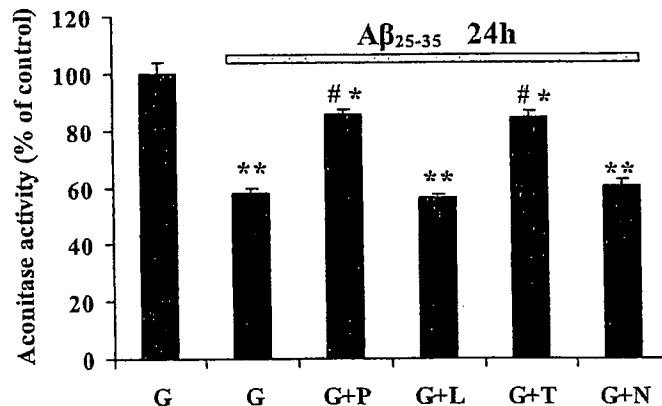

FIG. 4. The protective effect of pyruvate on aconitase activity in hippocampal slices treated with $A\beta_{25-35}$ (40 μM) for 24 h. The results are expressed as a percentage of the aconitase activity measured at the end of incubation in the absence of $A\beta_{25-35}$ (control: 46.91 ± 3.83 nmol/mg protein; $n = 12$). In the presence of $A\beta_{25-35}$ (40 μM), G, G + P, G + L, G + T and G + N decreased aconitase activity in comparison with the control. In comparison to G, G + P and G + T increased aconitase activity, but G + L and G + N did not. Vertical bars indicate SEM, $n = 12$. Asterisks: significant differences from the control ($*P < 0.05$, $**P < 0.01$); # significant differences from the glucose treatment in the presence of $A\beta_{25-35}$ (40 μM) only at $P < 0.05$ by ANOVA ($F_{5,66} = 180.365$) followed by the Fisher's PLSD *post-hoc* test.

hippocampal slices in the presence of Aβ and explored the correlation between neuronal cell death and NAD^+ levels. We found that in comparison with the control group (glucose 10 mM,
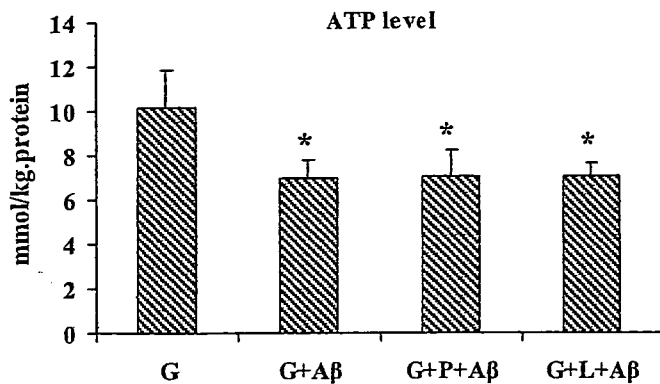
FIG. 5. Effect of MCTs on ATP levels in hippocampal slices treated with $A\beta_{25-35}$ (40 μM). In comparison to G (glucose: 10 mM), G +Aβ, G + P (5 mM) + Aβ and G + L (5 mM) + Aβ decreased ATP levels. No significant difference was observed among the G +Aβ, G +P +Aβ and G +L + Aβ groups. Vertical bars indicate SEM, $n = 12$. *Significant differences from glucose group at $P < 0.05$ by ANOVA ($F_{3,44} = 45.222$) followed by Fisher's PLSD post-hoc test.

6.5 ± 0.89 nmol/mg protein), glucose + pyruvate, but not glucose + lactate, increased the NAD^+ levels in the culture slices at 24 h by 16.4 ± 0.23% ($P < 0.05$). Exposure to 40 μM $A\beta_{25-35}$ for 24 h induced a significant decrease in NAD^+ levels with glucose, glucose + lactate and glucose + trolox condition ($P < 0.05$). In the presence of $A\beta_{25-35}$, the NAD^+ levels of the slices was kept above control levels (glucose) only in the glucose + pyruvate and glucose + niacinamide conditions (Fig. 6A). Trolox is a vitamin E analogue, which demonstrated a strong protective effect against Aβ neurotoxicity. Its protective effect did not correlate with the NAD^+ levels (Figs 2B and 6B), but it may instead be associated with its action as an ROS scavenger (Gibson et al., 2000). These results demonstrate that the neuronal cell death partially correlated with a decrease in NAD^+ levels in the hippocammpal organotypic slice cultures, and the supplementation of glucose-containing culture media with pyruvate, but not lactate, could protect neurons against Aβ-induced neurotoxicity by increasing the NAD^+ levels.

ATP and NAD⁺ levels before neuronal cell death

To assess the impact of the ATP and NAD^+ levels on the neuronal cell death by Aβ, experiments were performed at an early time point in treatment with 40 μM $A\beta_{25-35}$, when neuronal viability was still well maintained. Exposure to 40 μM $A\beta_{25-35}$ for 6 h did not induce cell death in each treatment (Fig. 7A). Incubation with 40 μM $A\beta_{25-35}$ for 6 h caused a significant decrease of ATP levels in the glucose (11.0 ± 0.55 mmol/kg protein), MCTs alone and glucose + MCTs groups in comparison with the control group (10 mM glucose) ($P < 0.05$, Fig. 7B). NAD^+ levels of the cultured slices decreased under glucose and and glucose + lactate by 19.8 ± 5.5 and 19.4 ± 4.3%, respectively ($P < 0.05$). However, the NAD^+ levels of the glucose + pyruvate group slices were maintained at 105.3 ± 14.1% of the control condition (Fig. 7C). These results suggest that Aβ causes a loss of NAD^+ and ATP levels before neuronal cell death in the hippocampal slice cultures.

Discussion

We found that pyruvate and lactate alone cannot replace glucose as an alternative energy source to preserve neuronal viability in hippocam-
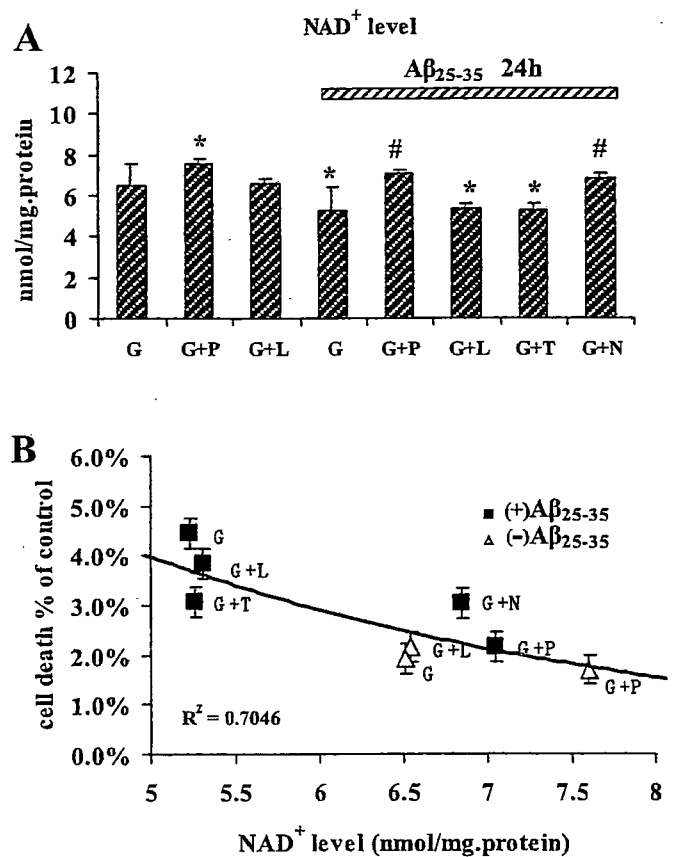

FIG. 6. (A) Effects of supplementation of the glucose-containing culture media with pyruvate (P: 5 mM) and lactate (L: 5 mM) on NAD^+ levels in hippocammpal organotypic slice cultures and with pyruvate (P: 5 mM), lactate (L: 5 mM), niacinamide (N: 10 mM) and trolox (T: 1 mM) on NAD^+ levels in the presence of $A\beta_{25-35}$ (40 μM). In comparison to the control (G: 10 mM), G + P increased the NAD^+ level, but G + L did not. In the presence of $A\beta_{25-35}$ (40 μM), G decreased the NAD^+ level in comparison to the control. In comparison to G, both G + P and G + N increased the NAD^+ levels, and G + T and G + L showed no significant differences. Vertical bars indicate SEM, $n = 12$. *Significant differences from the control; #significant differences from the glucose treatment in the presence of $A\beta_{25-35}$ (40 μM) only at $P < 0.05$ by ANOVA ($F_{7,88} = 35.121$) followed by Fisher's PLSD post-hoc test. (B) The negative correlation between the percentage of cell death and NAD^+ levels in hippocammpal organotypic slice cultures ($R^2 = 0.7046$).

pal slice cultures, and alone they cannot ameliorate Aβ neurotoxicity. In addition, the supplementation of glucose-containing culture media with pyruvate, but not lactate, improves neuronal survival in hippocampal slice cultures and also protects neurons against Aβ-induced cell death.

Although glucose is generally considered to be the main substrate to maintain neural activity in the central nervous system, the brain can utilize alternative metabolic substrates such as MCTs to sustain brain function when glucose is unavailable (Agardh et al., 1981). MCT is an essential route for the supply of the energy substrate to neurons during glucose deprivation (Cater et al., 2001) and endogenous MCT rather than glucose maintains neuronal integrity during energy deprivation (Izumi et al., 1997). However, we herein show that pyruvate and lactate alone cannot replace glucose as an alternative energy source to preserve neuronal viability in hippocampal slice cultures (Figs 1A and 3), although they can preserve ATP levels (data not shown). Okada (1982) also found that although the addition of either lactate or pyruvate instead of glucose maintained the original levels of ATP and
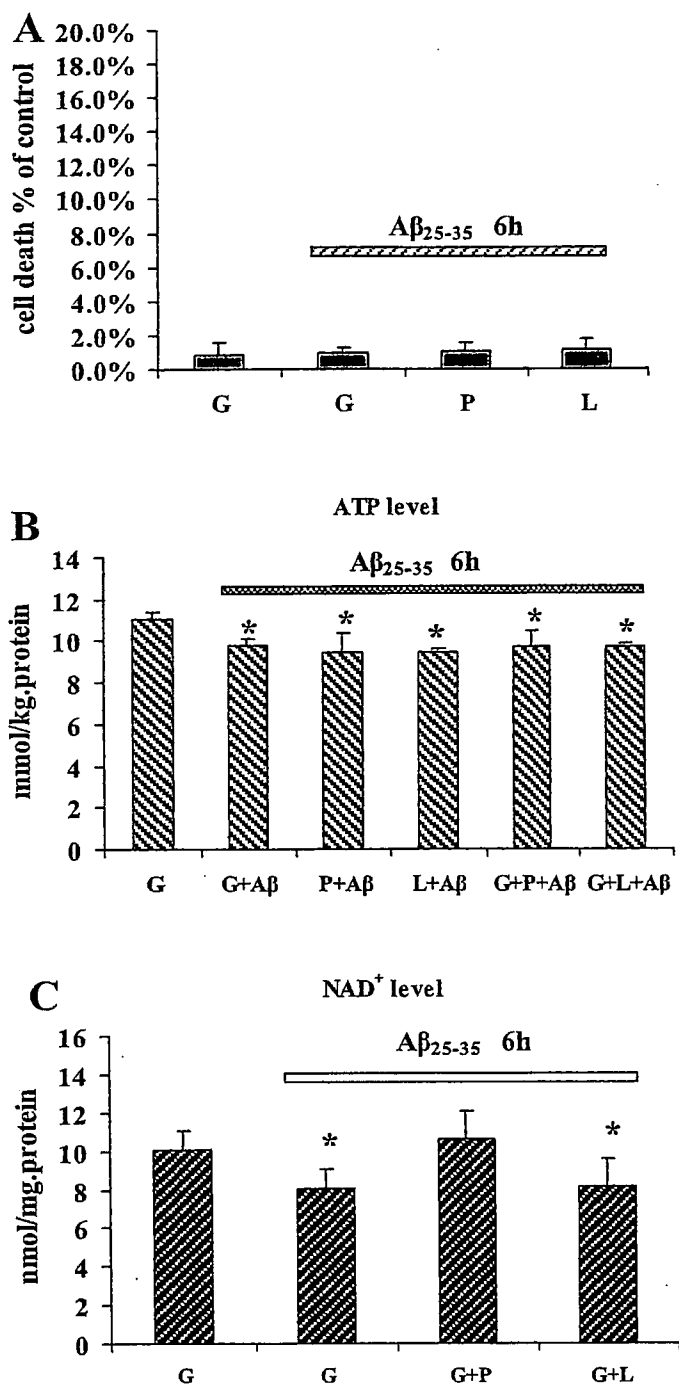
FIG. 7. Changes in cell death, ATP levels and NAD^+ levels in hippocampal slices in the presence of $A\beta_{25-35}$ (40 μM) at 6 h. (A) Incubation with $A\beta_{25-35}$ (40 μM) for 6 h did not cause neuron death in each treatment. (B) Incubation with $A\beta_{25-35}$ (40 μM) for 6 h decreased the ATP levels in each treatment [*P < 0.05 vs. G in the absence of $A\beta_{25-35}$, ANOVA ($F_{5,66}$ = 17.555) followed by Fisher's PLSD *post-hoc* test]; no significant difference was observed among these treatments. (C) In the presence of $A\beta_{25-35}$ (40 μM) at 6 h, G and G + L decreased the NAD^+ levels [*P < 0.05 vs. G in the absence of $A\beta_{25-35}$, ANOVA ($F_{3,44}$ = 21.920) followed by Fisher's PLSD *post-hoc* test], and G + P showed no significant difference. Vertical bars indicate SEM, n = 12.

CrP, neural activity was diminished over time as in glucose deprivation. Some reports have shown that glycolytically generated ATP is necessary for various phosphorylation reactions. Silver &

Erencinska (1997) reported that glycolysis generation of ATP was required for sodium pump activity in cultured murine cortical neurons and Xu *et al.* (1995) showed that ATP generated from glycolysis played an important role in regulating Ca^{2+} homeostasis via the calcium pump in the sarcoplasmic reticulum. These results strongly suggest that the presence of glucose is essential in the maintenance of both neuronal function and survival, and its requirement is not simply explained by its role as the energy substrate.

Furthermore, we found that supplementation of glucose-containing culture media with pyruvate improved neuronal survival in hippocampal slice cultures (Fig. 3E), but not with lactate, although they have the same effect on the maintenance of ATP levels in cultured slices (data not shown). Based on *in vitro* studies using primary cell cultures, several reports have described the protective effect of pyruvate against cell toxicity. The supplementation of glucose-containing culture media with pyruvate plus malate protects rat primary neurons from Aβ-induced degeneration and cell death (Alvarez *et al.*, 2003). Pyruvate potently protects against zinc toxicity in cultured rat retinal cells (Yoo *et al.*, 2004) and limits zinc-induced rat oligodendrocyte progenitor cell death (Kelland *et al.*, 2004). Pyruvate also protects neurons against hydrogen peroxide-induced toxicity (Desagher *et al.*, 1997). These protective effects of pyruvate have not yet been explored in detail by a more complex structure and *in vivo*-like system, such as a slice culture system. Using hippocampal slice cultures, we examined the effect of MCTs (particularly pyruvate and lactate) on Aβ-induced neuronal neurotoxicity. We found that pyruvate and lactate alone could not ameliorate Aβ neurotoxicity (Fig. 1B), but that supplementation of glucose-containing culture media with pyruvate could ameliorate Aβ neurotoxicity to levels as strong as with trolox, a known ROS scavenger, and niacinamide, an NAD^+ precursor. Lactate, by contrast, which can be used as a neuronal energy substrate as well as pyruvate, failed to protect against Aβ neurotoxicity (Fig. 2B). Aβ is known to decrease the ATP levels of cells (Zhang *et al.*, 1996). Our finding that neither pyruvate nor lactate ameliorated the decrease of ATP levels induced by Aβ in the glucose-containing culture media demonstrates that the protective effect of pyruvate cannot be explained by its role as an energy substrate.

Cell toxicity by Aβ has been demonstrated via oxidative stress (Mark *et al.*, 1996) or indirectly through intracellular production of ROS (Behl *et al.*, 1994; Schubert *et al.*, 1995) and protected by antioxidants (Pereira *et al.*, 1999). Pyruvate has been shown to function as an effective antioxidant directly by its capacity to reduce hydrogen peroxide to water and indirectly by increasing the levels of reduced glutathione rather than as providing an improvement in energy metabolism (Crestanello *et al.*, 1995; Bassenge *et al.*, 2000; Mohanty *et al.*, 2002). The Krebs-cycle enzyme aconitase is extremely sensitive to free radicals; superoxide (Patel *et al.*, 1996) or hydrogen peroxide at micromolar concentrations induces significant inactivation of the enzyme (Tretter *et al.*, 2000). Therefore, it can be used as a sensitive marker of ROS formation. In the present paper, we observed that aconitase activity was significantly reduced after incubation for 24 h with 40 μM $A\beta_{25-35}$, and that the loss of aconitase activity was restored by addition of 5 mM pyruvate and 1 mM trolox, the latter being a known ROS scavenger (Fig. 4). We herein also showed that the supplementation of glucose-containing culture media with pyruvate protected neurons from cell death to levels as strong as with the vitamin E analogue trolox (Fig. 2). These results indicate that the supplementation of glucose-containing culture media with pyruvate could protect neurons against Aβ-induced cell death through reducing ROS accumulation. A subset of Aβ plaques produces free radicals (ROS) in the brain tissues of AD patients (McLellan *et al.*, 2003) and Aβ has also been reported to increase the generation of ROS, which in

turn inactivates aconitase (Longo *et al.*, 2000). Whether the aconitase activity is suppressed in the AD brain *in vivo* has not yet been clarified; however, its activity has been shown to be severely depleted in the brains of patients with certain severe neurological disorders such as Huntington's disease (Shapira, 1999).

Exposure to $A\beta_{25-35}$ induced an early fall in NAD^+ levels before the initiation of cell death (Fig. 7A and C). NAD^+ is necessary for cell survival and it participates in a variety of essential metabolic processes including DNA repair, cell signaling and as a cofactor for a number of dehydrogenase enzymes. The depletion of NAD^+ levels disturbs metabolism of glucose, and in settings where glucose is the main metabolic substrate, it leads to mitochondrial dysfunction and cell death (Ying *et al.*, 2003; Alano *et al.*, 2004). Memory deficits in AD have been reported to improve following NAD^+ administration (Birkmayer, 1996) and the increased NAD^+ levels in the brain have been demonstrated to prevent AD-type $A\beta$ neuropathology through the activation of Sirtuin1 (Qin *et al.*, 2006). Exogenous pyruvate helps replenish NAD^+ from NADH by its conversion to lactate via lactate dehydrogenase. In addition to replenishing the NAD^+ needed for glycolysis, exogenous pyruvate also serves as a direct TCA cycle substrate.

In the present study, we first report that the supplementation of glucose-containing culture media with pyruvate, but not lactate, has a neuroprotective effect against $A\beta$-induced neurotoxicity in hippocampal slices and that this protective effect would be through both ROS scavenging and NAD^+ production. In addition, as pyruvate can cross the blood–brain barrier (Oldendorf, 1973), it could be of therapeutic value in pathological situations such as ischemia-reperfusion or trauma, in which the acute production of free radicals is believed to play a critical role (Desagher *et al.*, 1997). Considering the low cost and small number of side-effects associated with pyruvate, its application as a neuroprotective drug is expected to provide good cost-effectiveness in the clinical treatment of CNS vascular and degenerative disease, especially for the treatment of AD as a ROS scavenger and through enhancement of NAD^+ levels.

Abbreviations

AD, Alzheimer's disease; $A\beta$, amyloid β-peptide; 4-CIN, α-cyano-4-hydroxy-cinnamic acid; MCTs, monocarboxylates; NAD^+, nicotinamide adenine dinucleotide; ROS, reactive oxygen species; PI, propidium iodide.

References

Agardh, C.D., Chapman, A.G., Nilsson, B. & Siesjo, B.K. (1981) Endogenous substrates utilized by rat brain in severe insulin-induced hypoglycemia. *J. Neurochem.*, 36, 490–500.

Alano, C.C., Ying, W. & Swanson, R.A. (2004) Poly (ADP-ribose) polymerase-1-mediatated cell death in astrocytes requires NAD (+) depletion and mitochondrial permeability transition. *J. Biol. Chem.*, 279, 18895–18902.

Alvarez, G., Ramos, M., Ruiz, F., Satrústegui, J. & Bogónez, E. (2003) Pyruvate protection against β-Amyloid-induced neuronal death: role of mitochondrial redox state. *J. Neurosci. Res.*, 73, 260–269.

Bassenge, E., Sommer, O., Schwemmer, M. & Bunger, R. (2000) Antioxidant pyruvate inhibits cardiac formation of reactive oxygen species through changes in redox state. *Am. J. Physiol.*, 279, H2431–H2438.

Behl, C., Davis, J.B., Lesley, R. & Schubert, D. (1994) Hydrogen peroxide mediates amyloid beta protein toxicity. *Cell*, 77, 817–827.

Birkmayer, J.G. (1996) Coenzyme nicotinamide adenine dinucleotide: new therapeutic approach for improving dementia of the Alzheimer type. *Ann. Clin. Lab. Sci.*, 26, 1–9.

Cater, H.L., Benham, C.D. & Sundstrom, L.E. (2001) Neuroprotective role of monocarboxylate transport during glucose deprivation in slice cultures of rat hippocampus. *J. Physiol.*, 531, 459–466.

Crestanello, J.A., Kamelgard, J. & Whitman, G.J. (1995) The cumulative nature of pyruvate's dual mechanish for myocardial protection. *J. Surg. Res.*, 59, 198–204.

Desagher, S., Glowinski, J. & Premont, J. (1997) Pyruvate protects neurons against hydrogen peroxide-induced toxicity. *J. Neurosci.*, 17, 9060–9067.

Gibson, G.E., Zhang, H., Sheu, K.R. & Park, L.C.H. (2000) Differential alterations in antioxidant capacity in cells from Alzheimer patients. *Biochim. Biophys. Acta*, 1502, 319–329.

Izumi, Y., Katsuki, H. & Zorumski, C.F. (1997) Monocarboxylates (pyruvate and lactate) as alternative energy substrates for the induration of long-term potentiation in rat hippocampal slices. *Neurosci. Lett.*, 232, 17–20.

Kanatani, T., Mizuno, K. & Okada, Y. (1995) Effects of glycolytic metabolites on the preservation of high energy phosphate level and synaptic transmission in the granule cells of guinea pig hippocampal slices. *Experientia*, 51, 213–216.

Kelland, E.E., Kelly, M.D. & Toms, N.J. (2004) Pyruvate limits zinc-induced rat oligodendrocyte progenitor cell death. *Eur. J. Neurosci.*, 19, 287–294.

Lee, Y.J., Kang, I.J., Bunger, R. & Kang, Y.H. (2003) Mechanisms of pyruvate inhibition of oxidation-induced apoptosis in human endothelial cells. *Microvasc. Res.*, 66, 91–101.

Liang, L.P., Ho, Y.S. & Patel, M. (2000) Mitochondrial superoxide production in kainate-induced hippocampal damage. *Neuroscience*, 101, 563–570.

Longo, V.D., Viola, K.L., Klein, W.L. & Finch, C.E. (2000) Reversible inactivation of superoxide-sensitive acnitase in $A\beta_{1-42}$-treated neuronal cell lines. *J. Neurochem.*, 75, 1977–1985.

Macklis, J.D. & Madison, R.D. (1990) Progressive incorporation of propidium iodide in cultured mouse neurons correlates with declining electrophysiological status: a fluorescence scale of membrane integrity. *J. Neurosci. Meth.*, 31, 43–46.

Mark, R.J., Blanc, E.M. & Mattson, M.P. (1996) Amyloid β-Peptide and oxidative cellular injury in Alzheimer's disease. *Mol. Neurobiol.*, 12, 211–224.

Mattson, M.P. (1997) Cellular actions of beta-amyloid precursor protein and its soluble and fibrillogenic derivatives. *Physiol. Rev.*, 77, 1081–1132.

McLellan, M.E., Kajdasz, S.T., Hyman, B.T. & Bacskai, B.J. (2003) In vivo imaging of reactive oxygen species specifically associated with thioflavine S-positive amyloid plaques by multiphoton microscopy. *J. Neurosci.*, 23, 2212–2217.

Mohanty, I., Joshi, S., Trivedi, D., Srivastava, S., Tandon, R. & Gupta, S.K. (2002) Pyruvate modulates antioxidant status of cultured human lens epithelial cells under hypergalactosemic conditions. *Mol. Cell Biochem.*, 238, 129–135.

Okada, Y. (1974) Recovery of neuronal activity and high-energy compound level after complete and prolonged brain ischemia. *Brain Res.*, 72, 346–349.

Okada, Y. (1982) Reversibility of neuronal function of hippocampal slices during deprivation of oxygen and/or glucose. In Somjen, G.G. (Ed.), *Mechanism of Cerebral Hypoxia and Stroke*. Plenum Press, New York, 191–203.

Oldendorf, W.H. (1973) Carrier-mediated blood–brain barrier transport of short chain monocarboxylic organic acids. *Am. J. Physiol.*, 224, 1450–1453.

Patel, M., Day, B.J., Crapo, J.D., Fridovich, I. & McNamara, J.O. (1996) Requirement for superoxide in excitotoxic cell death. *Neuron*, 16, 345–355.

Pereira, C., Santos, M.S. & Oliveira, C. (1999) Involvement of oxidative stress on the impairment of energy metabolism induced by $A\beta$ peptides on PC 12 cells: protection by antioxidants. *Neurobiol. Dis.*, 6, 209–219.

Qin, W., Yang, T.H.O.L., Zhao, Z., Wang, J., Chen, L., Zhao, W., Thiyagarajan, M., Grogan, D.M., Rodgers, J.T., Puigserver, P., Sadoshima, J., Deng, H., Pedrini, S., Gandy, S., Sauve, A.A. & Pasinetti, G.M. (2006) Neuronal SIRT1 activation as a novel mechanism underlying the prevention of Alzheimer disease amyloid neuropathology by calorie restriction. *J. Biol. Chem.*, 281, 21745–21754.

Roberts, E.L. Jr (1993) Glycolysis and recovery of potassium ion homeostasis and synaptic transmission in hippocampal slices after anoxia or stimulated potassium release. *Brain Res.*, 620, 251–257.

Roselli, F., Tirard, M., Lu, J., Hutzler, P., Lambert, i, P., Livrea, P., Morabito, M. & Almeida, O.F.X. (2005) Soluble β-Amyloid$_{1-40}$ induces NMDA-dependent degradation of postsynaptic density-95 at glutamatergic synapses. *J. Neurosci.*, 25, 11061–11070.

Sander, B.J., Oelshlegel, F.J. Jr & Brewer, G.J. (1976) Quantitative analysis of pyridine nucleotides in and blood cells: a single-step extraction procedure. *Anal. Biochem.*, 71, 29–36.

Schubert, D., Behl, C., Lesley, R., Brack, A., Dárgusch, R., Sagara, Y. & Kimura, H. (1995) Amyloid peptides are toxic via a common oxidative mechanism. *Proc. Natl Acad. Sci. USA*, 92, 1989–1993.

Schurr, A., West, C.A. & Rigor, B.M. (1988) Lactate-supported synaptic function in the rat hippocampal slice preparation. *Science*, **240**, 1326–1328.

Shapira, A.H. (1999) Mitochondrial involvement in Parkinson's disease, Hungtington's disease and hereditary spastic paraplegia and Friedreich's ataxia. *Biochim. Biophys. Acta*, **1410**, 99–102.

Sheline, C.T., Behrens, M.M. & Choi, D.W. (2000) Zinc-induced cortical neuronal death: contribution of energy failure attributable to loss of NAD$^+$ and inhibition of glycolysis. *J. Neurosci.*, **20**, 3139–3146.

Silver, I.A. & Erencinska, M. (1997) Ion homeostasis in brain cells: differences in intracellular ion response to energy limitation between cultured neurons and glial cells. *Neuroscience*, **78**, 589–601.

Sipos, I., Tretter, L. & Adam-Vizi, V. (2003) Quantitative relationship between inhibition of respiratory complexes and formation of reactive oxygen species in isolated nerve terminals. *J. Neurochem.*, **84**, 112–118.

Stoppini, L., Buchs, P.A. & Muller, D. (1991) A simple method for organotypic cultures of nervous tissue. *J. Neurosci. Meth.*, **37**, 173–182.

Takata, T. & Okada, Y. (1995) Effects of deprivation of oxygen or glucose on the neural activity in the guinea pig hippocampal slice-intracellular recording study of pyramidal neurons. *Brain Res.*, **683**, 109–116.

Takata, T., Sakurai, T., Yokono, K. & Okada, Y. (2001) Effect of lactate on the synaptic potential energy metabolism calcium homeostasis and extra cellular glutamate concentration in the dentate gyrus of the hippocampus from guinea-pig. *Neuroscience*, **104**, 371–378.

Takata, T., Yang, B., Sakurai, T., Okada, Y. & Yokono, K. (2004) Glycolysis regulates the inducation of lactate utilization for synaptic potential after hypoxia in the granule cell of guinea pig hippocampus. *Neuurosci. Res.*, **50**, 467–474.

Tilton, W.M., Seaman, C., Carriero, D. & Piomolli, S. (1991) Regulation of glycosis in the erythrocyte: role of the lactate/pyruvate and NAD/NADH ratios. *J. Lab. Clin. Med.*, **118**, 146–152.

Tretter, L. & Adam-Vizi, V. (2000) Inhibition of Krebs cycle enzymes by hydrogen peroxide: a key role of α-ketoglutarate dehydrogenase in limiting NADH production under oxidative stress. *J. Neurosci.*, **20**, 8972–8979.

Tretter, L., Liktor, B. & Adam-Vizi, V. (2005) Dual effect of pyruvate in isolated nerve terminals: generation of reactive oxygen species and protection of aconitase. *Neurochem. Res.*, **30**, 1331–1338.

Wada, H., Okada, Y., Nabetani, M. & Nakamura, H. (1997) The effects of lactate and β-hydroxybutyrate on the energy metabolism and neural activity of hippocampal slices from adult and immature rat. *Brain Res. Dev. Brain Res.*, **101**, 1–7.

Xu, K.Y., Zweier, J.L. & Becker, L.C. (1995) Functional coupling between glycolysis and sarcoplasmic reticulum Ca^{2+} transport. *Circ. Res.*, **77**, 88–97.

Yanagisawa, K. (2000) Neuronal death in Alzheimer's disease. *Int. Med.*, **39**, 328–330.

Ying, W., Garnier, P. & Swanson, R.A. (2003) NAD (+) repletion prevents PARP-1-induced glycolytic blockade and cell death in cultured mouse astrocytes. *Biochem. Biophys. Res. Commun.*, **308**, 809–813.

Yoo, M.H., Lee, G.Y., Lee, S.E., Koh, J.Y. & Yoon, Y.H. (2004) Protection by pyruvate of rat retinal cell against zinc toxicity in vitro and pressure-induced ischemia in vitro. *Invest. Ophthalmol. Vis. Sci.*, **45**, 1523–1530.

Zhang, Z., Rydel, R.E., Drzewiecki, G.J., Fuson, K., Wright, S., Wogulis, M., Audia, J.E., May, P.C. & Hyslop, P.A. (1996) Amyloid beta-mediated oxidative and metabolic stress in rat cortical neurons: no direct evidence for a role for H$_2$O$_2$ generation. *J. Neurochem.*, **67**, 1595–1606.

Factors associated with lower mini mental state examination scores in elderly Japanese diabetes mellitus patients

Hiroyuki Umegaki [a,*], Satoshi Iimuro [b], Tetsuji Kaneko [c], Atsushi Araki [d], Takashi Sakurai [e], Yasuo Ohashi [c], Akihisa Iguchi [a], Hideki Ito [f]

[a] *Department of Geriatrics, Nagoya University Graduate School of Medicine, 65 Tsuruma-Cho, Showa-Ku, Nagoya, Aichi 466-8550, Japan*
[b] *Department of Cardiovascular Medicine, Graduate School of Medicine, University of Tokyo, Tokyo, Japan*
[c] *Department of Biostatistics, School of Health Sciences and Nursing, University of Tokyo, Tokyo, Japan*
[d] *Department of Endocrinological Medicine, Tokyo Metropolitan Geriatric Medical Center, Tokyo, Japan*
[e] *Department of Internal and Geriatric Medicine, Kobe University Graduate School of Medicine, Kobe, Japan*
[f] *Tokyo Metropolitan Geriatric Medical Center, Tokyo, Japan*

Abstract

Cognitive impairment in elderly diabetic patients has generated considerable interest recently; however, the mechanism of the impairment remains to be elucidated. In the current study, factors associated with cognitive dysfunction in old diabetic patients were explored. A Mini Mental State Examination (MMSE) was performed on 907 of 1173 registered elderly Japanese diabetic subjects. To characterize the clinical features of diabetes, we examined indices of glycemic control, lipid metabolism, blood pressure and complications. Single regression analysis adjusted for age showed that shorter height, higher GDS 15 scores, lower serum albumin, history of cerebrovascular disease, the existence of diabetic nephropathy, no smoking habit, no drinking habit, and no occupation were associated with lower MMSE scores. Multiple regression analysis demonstrated that age (odds ratio (OR) = 1.079; 95% confidence interval (CI) = 1.011–1.150), GDS 15 scores (OR = 1.139; 95% CI = 1.045–1.243), serum albumin (OR = 0.336; 95% CI = 0.174–0.745), and history of cerebrovascular disease (OR = 3.011; 95% CI = 1.578–5.748) were the variables significantly associated with having lower MMSE scores.
© 2007 Elsevier Inc. All rights reserved.

Keywords: Cognition; Dementia; Serum albumin; Cerebrovascular accident; Depression

1. Introduction

The prevalence and incidence of diabetes mellitus (DM) are increasing at all ages, including older populations, and approximately 15% of the elderly population in Japan is affected. Multiple metabolic abnormalities in DM induce systemic complications, which may include microangiopathic complications (neuropathy, retinopathy, nephropathy) and macroangiopathic atherosclerosis (stroke and ischemic heart disease). Several studies have shown that elderly diabetics have impaired cognition compared to age-matched non-diabetics, as well as a higher risk of dementia (Cukierman et al., 2005; Mogi et al., 2004; Strachen et al., 1997). Because the increase in the number of elderly people with cognitive impairment or dementia creates significant medical, social and economic burdens, cognitive impairment in older DM subjects has recently sparked considerable interest. It is highly desirable to be able to provide intervention in the case of older DM subjects who are at risk for cognitive decline or dementia in order to preserve cognitive functions; however, the mechanism of DM-associated cognitive decline remains to be elucidated and there is no solid evidence as yet that any treatment for DM is effective in preventing cognitive decline (Areosa Sastre and Grimley Evans, 2007).

* Corresponding author. Tel.: +81 52 744 2365; fax: +81 52 744 2371.
E-mail address: umegaki@med.nagoya-u.ac.jp (H. Umegaki).

In order to establish an effective way of treating or preventing DM-related cognitive decline, the factors associated with this condition must first be determined. In the present study, we investigated factors associated with cognitive impairment in elderly DM subjects using baseline data from a large-scale cohort study of elderly DM in Japan.

2. Methods

2.1. Participants

The J-EDIT study was initiated in 2001 as a prospective intervention study of elderly Japanese people with DM for the purpose of determining how to prevent several diabetic complications. One thousand one hundred and seventy-three diabetic subjects were enrolled in 39 institutes and hospitals in Japan. They were all aged 65 years or more and had serum HbA1c levels at least 7.5%, or at least 7.0% with one of the following comorbidity factors: hypertension (130/85 mmHg and over), obesity (a body mass index (BMI) of at least 25), dyslipidemia (total cholesterol of at least 200 mg/dl, low-density lipoprotein (LDL) of at least 120 mg/dl, high-density lipoprotein (HDL) of 40 mg/dl or less, and/or triglyceride of at least 150 mg/dl). Although no exclusion criteria were determined for the registration of JEDIT, severely demented subjects were not selected because the filling out of several questionnaires was mandatory.

The study protocol was approved by the ethical committee in all of the enrolled institutes, and written informed consent was obtained from each patient.

2.2. Functional assessment

The Mini Mental State Examination (MMSE) was administered to most patients (907 of 1173) upon registration (Folstein et al., 1978). The MMSE is a global test of orientation, attention, calculation, language and recall with a score of 0–30.

Of the 1173 enrolled cases, MMSE scores were not collected in 266; data sheets were not returned in 48, subjects dropped out just after registration in 35, and doctors did not perform MMSE in 183.

Basic activities of daily living (BADL) was measured by a Barthel Index score of 0–20 (Mahoney and Barthel, 1965), and depressive mood was assessed by a short version of the Geriatric Depression Scale (GDS-15) (Yesavage, 1986).

2.3. Assessment of diabetes mellitus, complications and comorbidities

The diagnosis and patient data regarding DM, blood examinations and complications were obtained from clinical charts (The Expert Committee, 2003). After overnight fasting, blood samples were taken by venipuncture to assess serum levels of glucose, HbA1c, total cholesterol, triglyceride and HDL

cholesterol. Additionally, serum insulin concentrations were determined in patients who were not receiving insulin therapy. Diabetic nephropathy was assessed according to the mean urinary albumin-to-creatinine ratio (ACR) and was classified as no nephropathy (ACR < 30 μg/mg) or existence of nephropathy (microalbuminemia: 30 ACR < 300 μg/mg or more advanced). Diabetic retinopathy was assessed by fundoscopic examination performed through dilated pupils by experienced ophthalmologists, and was classified into two categories: mild (no retinopathy or intraretinal hemorrhages and hard exudates), or serious (soft exudates, intraretinal microvascular abnormalities, venous calibre abnormalities, venous beading, neovascularization of the disc or other areas in the retina, preretinal fibrous tissue proliferation, preretinal or vitreous hemorrhage, and/or retinal detachment). Diabetic neuropathy was defined as either the loss of the Achilles tendon reflex without neuropathic symptoms including paresthesia, or the presence of neuropathic symptoms. Macrovascular complications were classified based on the presence or absence of coronary artery diseases, and/or a history of stroke. The existence of a current regular occupation and current habits of smoking, drinking and exercising were also assessed by questionnaire as yes (1) or no (0).

2.4. Statistical analysis

The subjects were divided into two groups, one with higher cognitive function, defined as having an MMSE score of 24 or more, and one with lower cognitive function, defined as having an MMSE score of 23 or less, according to the review by Tombaugh and McIntyre (1992). The groups were compared with respect to each factor by the Student's t-test for continuous variables or a χ^2-test for categorical variables. Logistic regression analysis including each factor as an explanatory variable was performed to search the association of the covariants and cognitive dysfunction indicated by an MMSE score below 24 after adjusting for age. Then, multiple logistic regression analysis was performed with the variables selected by this analysis and additional variables of interest. Spearman's rank correlation coefficient was calculated to confirm the relationship between serum albumin levels and MMSE scores.

3. Results

The background characteristics of the two MMSE score groups are shown in Tables 1 and 2. The average age was 74.0 years old in the lower MMSE-score group (23 and less) and 71.8 years old in the higher MMSE-score group (24 and more) (Table 1). The average HbA1c and FBG levels in the higher MMSE score group and lower MMSE score group were 8.0% versus 8.1% and 5.1 mmol/l versus 5.0 mmol/l, respectively (Table 1). At least about half of the participants had microangiopathic complications (nephropathy, retinopathy, or neuropathy) as shown in Table 2.

Table 1
Analysis by Student's t-test

Item	Higher	Lower	p-Value
Number	848	59	
Age (years)	71.8 ± 4.6	74.0 ± 5.1	<0.001
DM duration (years)	16.3 ± 9.7	17.1 ± 8.8	0.545
Height (cm)	155.8 ± 8.4	152.3 ± 8.6	0.002
Body weight (kg)	57.9 ± 10.2	57.7 ± 8.8	0.071
BMI	23.8 ± 3.5	23.9 ± 3.2	0.874
HbA1c (%)	8.0 ± 0.9	8.1 ± 1.1	0.766
FBG (mmol/l)	5.1 ± 0.3	5.0 ± 0.5	0.234
Systolic BP (mmHg)	135.4 ± 15.6	133.3 ± 19.3	0.391
Diastolic BP (mmHg)	74.9 ± 9.5	76.4 ± 11.2	0.288
LDL cholesterol (mg/dl)	120.9 ± 30.6	126.2 ± 35.7	0.201
HDL cholesterol (mg/dl)	56.4 ± 18.0	57.7 ± 18.4	0.567
Triglyceride (log)	4.7 ± 0.5	4.6 ± 0.5	0.353
Lp (a) (mg/dl)	23.1 ± 22.9	25.9 ± 23.5	0.362
Albumin (g/dl)	4.2 ± 0.4	4.1 ± 0.5	0.001
MMSE	28.5 ± 1.8	20.3 ± 3.0	<0.001
ADL	19.9 ± 3.4	18.9 ± 1.0	<0.001
GDS-15	4.0 ± 3.1	5.9 ± 3.9	<0.001

Higher: the group with higher MMSE scores (24 or more), Lower: the group with lower MMSE scores (23 or less).

Analysis by Student's t-test showed that age, height, activities of daily living (ADL) scores, and serum albumin were significantly different between the two groups of patients (Table 1). A history of cerebrovascular disease, existence of diabetic nephropathy, current smoking habit, current drinking habit, and absence of occupation were also demonstrated to have a significantly different distribution between the two groups (Table 2). Fasting serum insulin levels or insulin treatment were not significantly associated with MMSE scores.

To determine variables significantly associated with cognitive dysfunction, logistic regression analysis adjusted for age was performed. The variables selected by this analysis were age, body height, serum albumin, the existence of an occupation, smoking habits, drinking habits, the existence of nephropathy, GDS-15 scores and history of cerebrovascular disease (Table 3). Then, multiple regression analysis was performed with all these significant variables plus variables of

Table 2
Analysis by χ^2-test

	Higher	Lower	p-Value
Male	45.9 (389)	40.0 (23)	0.304
Existence of current occupation	67.2 (552)	47.4 (27)	0.002
Existence of exercise habit	61.1 (497)	48.3 (28)	0.055
Current drinking habit	40.4 (343)	25.4 (15)	0.017
Current smoking habit	46.5 (383)	31.0 (18)	0.022
Existence of nephropathy	48.5 (411)	64.4 (38)	0.018
Existence of retinopathy	48.8 (413)	60.8 (35)	0.088
Existence of neuropathy	65.5 (544)	73.2 (41)	0.241
User of antihypertensive drugs	55.2 (468)	62.7 (37)	0.261
User of antidyslipidemic drugs	38.8 (329)	42.4 (25)	0.586
Antiplatlet user	26.9 (227)	49.2 (29)	<0.001
Presence of IHD	17.6 (149)	16.3 (9)	0.650
History of cerebrovascular disease	12.6 (107)	32.2 (19)	<0.001

Higher: the group with higher MMSE scores (24 or more). Lower: the group with lower MMSE scores (23 or less). Data are expressed as percentages of the total with the number in parentheses.

Table 3
Univariate regression analysis adjusted with age

	Odds ratio	95% CI	p-Value
Height (cm)	0.959	0.928–0.992	0.015
Gender (male)	1.232	0.714–2.126	0.453
HbA1c (%)	1.033	0.779–1.369	0.822
Systolic blood pressure (mmHg)	1.005	0.988–1.021	0.576
Diastolic blood pressure (mmHg)	1.017	0.990–1.044	0.230
Albumin (g/dl)	0.322	0.163–0.637	0.001
History of cerebrovascular disease	3.128	1.735–5.637	<0.001
Existence of nephropathy	1.877	1.079–3.264	0.026
Existence of retinopathy	1.730	0.998–2.997	0.051
Existence of neuropathy	1.369	0.742–2.527	0.315
Existence of current occupation	0.498	0.287–0.863	0.013
Current drinking habit	0.527	0.287–0.968	0.039
Current smoking habit	0.544	0.305–0.968	0.038
GDS-15	1.166	1.080–1.259	<0.001
ADL	1.019	0.998–1.042	0.0810

95% CI: 95% confidence interval.

Table 4
Multiple logistic regression analysis

	Odds ratio	95% CI	p-Value
Age (years)	1.079	1.011–1.150	0.021
Height (cm)	0.954	0.905–1.006	0.083
Gender (male)	0.429	0.139–1.323	0.141
Albumin (g/dl)	0.336	0.174–0.745	0.006
HbA1c (%)	0.965	0.703–1.325	0.828
History of cerebrovascular disease	3.011	1.578–5.748	<0.001
Existence of nephropathy	1.679	0.913–3.089	0.096
Existence of current occupation	0.725	0.348–1.368	0.321
Current smoking habit	0.516	0.223–1.195	0.123
Current drinking habit	0.601	0.274–1.315	0.202
GDS-15 scores	1.139	1.045–1.243	0.003

95% CI: 95% confidence interval.

interest (HbA1c and gender) considered simultaneously. As shown in Table 4, higher age, higher GDS-15 scores, lower serum albumin and a history of cerebrovascular disease were significantly associated with the group having lower MMSE scores.

MMSE scores and serum albumin levels were significantly correlated based on Spearman's correlation (coefficient = 0.14902, $p < 0.001$).

4. Discussion

The analysis of the data from the J-EDIT study at registration demonstrated that a history of cerebrovascular disease, a low serum albumin level, higher GDS scores, and higher age were independently associated with lower cognitive function.

The present study demonstrated that in DM subjects, the strongest risk factor for cognitive dysfunction as defined by a MMSE score less than 24, which is considered to be the level defining dementia (Tombaugh and McIntyre, 1992), was a

history of stroke. Although the causes of cognitive dysfunction were not determined in the present study, vascular lesions might play a prominent role in the cognitive decline of DM subjects with a history of stroke. Furthermore, Snowdon et al. report that among subjects who met the neuropathological criteria for Alzheimer's disease, those with brain infarcts had poorer cognitive functions and a higher prevalence of dementia (Snowdon et al., 1997); thus, cerebrovascular disease might shorten the period of preclinical dementia. In the current study the participants were all Japanese, a race which is relatively prone to cerebrovascular diseases (Kitamura et al., 2006). The prevalence of a history of stroke in the current study was 13.9% (126 out of 907 participants), much higher than the 1.8% reported by Kuusisto et al. (1994) in Finland, and comparable to 18.8% in PROACTIVE, a secondary prevention study for macrovascular disease in diabetic patients performed in European countries (Charbonnel et al., 2004). Thus, the higher stroke prevalence might have affected the results of the current study.

Lower levels of serum albumin, even within the "normal" range, are associated with increased risks of stroke and coronary heart disease incidents as well as all-cause and cardiovascular mortality (Shaper et al., 2004). Of particular interest are several lines of evidence demonstrating that chronic inflammation is involved in atherosclerotic mechanisms, and high-serum proinflammatory factors including c-reactive protein, intereleukin-6 and tumor necrosis factor have been reported to be risk factors for progressed atherosclerosis; these proinflammatory factors reportedly suppress the synthesis of albumin in the liver (Chojkier, 2005). The present results indicate that lower serum albumin and a history of cerebrovascular disease are independent factors associated with cognitive decline. However, asymptomatic strokes may also be involved in the mechanism of cognitive impairment in elderly diabetic patients (Araki and Ito, 2002). Although lower serum albumin was strongly associated with cognitive decline, mean urinary ACR was not associated with MMSE scores (data not shown).

The scores of GDS-15, which assessed depressive mood, were significantly associated with lower MMSE scores. The association of a depressive mood with cognitive dysfunction has been reported (Jorm, 2000). However, the mechanism of this association remains to be elucidated (Jorm, 2000). Cognitive dysfunction and depression may share common risk factors, depression may be a risk factor or prodrome of cognitive dysfunction, depression may affect the threshold of cognitive dysfunction, or depression may be a causal factor in cognitive dysfunction. Further analysis of longitudinal data of JEDIT study may shed light on this subject.

Many population-based and clinical studies have shown that DM is associated with cognitive decline in the elderly (Cukierman et al., 2005; Mogi et al., 2004; Strachen et al., 1997). Several hypothetical mechanisms have been suggested for this impairment; however, their clinical relevance is unclear (Biessels et al., 2006). The J-EDIT study was an interventional prospective study with a randomized control design. Longitudinal clinical and cognitive assessment of elderly diabetic patients will provide more information on the mechanisms of DM-related cognitive disorders.

Some limitations should be considered in the present case. First, the present study was performed with cross-sectional design using the data obtained at registration for the J-EDIT study. The patients are being followed longitudinally, and a follow-up analysis will be reported in the future. Second, because all of the patients enrolled were diabetic, it was not clear whether or not the results of the present study were diabetes-specific. In particular, the involvement of low serum albumin in the mechanism of cognitive decline in non-diabetic elderly patients should be investigated. Third, the present study did not include brain imaging. A subgroup analysis of J-EDIT subjects who underwent brain magnetic resonance imaging (MRI) was recently reported elsewhere (Akisaki et al., 2006), and revealed that cognitive decline in diabetes was associated with white-matter hyperintensities and subcortical atrophy in the tested subgroup. However, the relationship between the present results and the results of MRI analysis requires further investigation.

In the present study, neither DM-specific clinical indices including HbA1c, fasting blood glucose and serum insulin level, nor DM-related microangiopathies (nephropathy, neuropathy, and retinopathy) were associated with lower MMSE scores. The J-EDIT study recruited patients with relatively severe DM status, and this group of patients therefore did not represent the general population of elderly diabetics. The criteria for diagnosis for microangiopathy in the present study were relatively simple. Retinopathy has been reported as being associated with cognitive impairment or brain atrophy (Musen et al., 2006; Wong et al., 2002); proteinuria, which is a symptom of diabetic nephropathy, has received attention as a risk for stroke and ischemic heart disease (Madison et al., 2006); dysfunctions of the central and peripheral nervous systems may share a common pathogenesis (Gispen and Biessel, 2000; Suzuki et al., 2006). Further investigation of subjects with a broader clinical background and more sensitive diagnostic criteria for DM-related microangiopathic complications is required.

In conclusion, based on the results obtained in the current cross-sectional assessment, the prevention of cerebrovascular disease may be a primary way of preventing cognitive decline in elderly DM subjects. An investigation of how lower serum albumin levels are associated with DM-related cognitive impairment may lead to the development of effective strategies for the prevention or treatment of this decline.

Conflict of interest declaration

There is no conflict of interest for any of the authors.

Acknowledgement

References

Areosa Sastre A., Grimley Evans J., 2007. Effects of treatment of type II diabetes mellitus on the development of cognitive impairment and dementia. The Cochrane Library, issue 2, http://www.cochrane.org/reviews/en/ab003804.html.

Akisaki, T., Sakurai, T., Takata, T., Umegaki, H., Araki, A., Mizuno, S., Tanaka, S., Ohashi, Y., Iguchi, A., Yokono, K., Ito, H., 2006. Cognitive dysfunction associates with white matter hyperintensities and subcortical atrophy on magnetic resonance imaging of the elderly diabetes mellitus Japanese Elderly Diabetes Intervention Trial (J-EDIT). Diabetes/Metab. Res. Rev. 22 (5), 376–384.

Araki, A., Ito, H., 2002. Asymptomatic cerebral infarction on brain MR images and cognitive function in elderly diabetic patients. Geriatr. Gerontol. Int. 2, 206–214.

Biessels, G.J., Staekenborg, S., Brunner, E., Brayne, C., Scheltens, P., 2006. Risk of dementia in diabetes mellitus: a systematic review. Lancet Neurol. 5, 64–74.

Charbonnel, B., Dormandy, J., Erdmann, E., Massi-Benedetti, M., Skene, A., PROactive Study Group, 2004. The prospective pioglitazone clinical trial in macrovascular events (PROactive) can pioglitazone reduce cardiovascular events in diabetes? Study design and baseline characteristics of 5238 patients. Diabetes Care 27, 1647–1653.

Chojkier, M., 2005. Inhibition of albumin synthesis in chronic diseases: molecular mechanisms. J. Clin. Gastroenterol. 39 (4 suppl. 2), S143–S146.

Cukierman, T., Gerstein, H.C., Williamson, J.D., 2005. Cognitive decline and dementia in diabetes-systematic overview of prospective observational studies. Diabetologia 48, 2460–2469.

Folstein, M.F., Folstein, S.E., McHigh, P.R., 1978. 'Mini-Mental State': a practical method of grading the cognitive function of patients for the clinician. J. Psychiatr. Res. 12, 189–198.

Gispen, W.H., Biessel, G.J., 2000. Cognition and synaptic plasticity in diabetes mellitus. Trends Neurosci. 23, 542–549.

Jorm, A.F., 2000. Is depression a risk factor for dementia or cognitive decline? A review. Gerontology 46, 219–227.

Kitamura, A., Nakagawa, Y., Sato, M., Iso, H., Sato, S., Imano, H., Kiyama, M., Okada, T., Okada, H., Iida, M., Shimamoto, T., 2006. Proportions of stroke subtypes among men and women 40 years of age in an urban Japanese city in 1992, 1997, and 2002. Stroke 37, 1374–1378.

Kuusisto, J., Mykkanen, L., Pyorala, K., Laakso, M., 1994. Non-insulin-dependent diabetes and its metabolic control are important predictors of stroke in elderly subjects. Stroke 6, 1157–1164.

Madison, J.R., Spies, C., Schatz, I.J., Masaki, K., Chen, R., Yano, K., Curb, J.D., 2006. Proteinuria and risk for stroke and coronary heart disease during 27 years of follow-up: the Honolulu Heart Program. Arch. Intern. Med. 166, 884–889.

Mahoney, F.I., Barthel, D.W., 1965. Functional evaluation: the Barthel Index. Md. State Med. J. 14, 61–65.

Mogi, N., Umegaki, H., Hattori, A., Maeda, N., Miura, H., Kuzuya, M., Shimokata, H., Ando, F., Ito, H., Iguchi, A., 2004. Cognitive function in Japanese elderly with type 2 diabetes mellitus. J. Diabetes Complict. 18 (1), 42–46.

Musen, G., Lyoo, I.K., Sparks, C.R., Weinger, K., Hwang, J., Ryan, C.M., Jimerson, D.C., Hennen, J., Renshaw, P.F., Jacobson, A.M., 2006. Effects of type 1 diabetes on gray matter density as measured by voxel-based morphometry. Diabetes 55, 326–333.

Shaper, A.G., Wannamethee, S.G., Whincup, P.H., 2004. Serum albumin and risk of stroke, coronary heart disease, and mortality: the role of cigarette smoking. J. Clin. Epidemiol. 57, 195–202.

Snowdon, D.A., Greiner, L.H., Mortimer, J.A., Riley, K.P., Greiner, P.A., Markesbery, W.R., 1997. Brain infarction and the clinical expression of Alzheimer disease. The Nun Study. JAMA 277 (10), 813–817.

Strachen, M.W., Ewing, F.M., Deary, I.J., et al., 1997. Is type 2 diabetes associated with an increased risk of cognitive dysfunction? A critical review of published studies. Diabetes Care 20, 438–445.

Suzuki, M., Umegaki, H., Ieda, S., Mogi, N., Iguchi, A., 2006. Factors associated with cognitive impairment in elderly diabetes mellitus patients. J. Am. Geriatr. Soc. 54, 558–559.

The Expert Committee on the Diagnosis and Classification of Diabetes Mellitus, 2003. Report of the expert committee on the diagnosis and classification of diabetes mellitus. Diabetes Care 26, S5–S20.

Tombaugh, T.N., McIntyre, N.J., 1992. The mini-mental state examination: a comprehensive review. J. Am. Geriatr. Soc. 40, 922–935.

Wong, T.Y., Klein, R., Sharrett, A.R., Nieto, F.J., Boland, L.L., Couper, D.J., Mosley, T.H., Klein, B.E., Hubbard, L.D., Szklo, M., 2002. Retinal microvascular abnormalities and cognitive impairment in middle-aged persons: the atherosclerosis risk in communities study. Stroke 33, 1487–1492.

Yesavage, J.A., 1986. The use of self-rating depression scales in the elderly. In: Poon, L.W. (Ed.), Clinical Memory Assessment of Older Adults. American Psychological Association, Washington, DC, pp. 213–217.

Proceedings of the 29th Annual International
Conference of the IEEE EMBS
Cité Internationale, Lyon, France
August 23-26, 2007.

FrD04.6

In Vivo Cerebral Artery Microangiography in Rat and Mouse Using Synchrotron Radiation Imaging System

Keiji Umetani, Keiji Kidoguchi, Akitsugu Morishita, Ximena-Sayuri Oizumi, Masahiro Tamaki,
Haruo Yamashita, Takashi Sakurai, and Takeshi Kondoh

Microangiography with spatial resolution in the micrometer range was carried out to depict vascular responses of the cerebral artery and arterioles in rats and mice using a real-time imaging system and a third generation synchrotron radiation source at SPring-8. An X-ray direct-conversion type detector with 6-μm spatial resolution was developed for real-time biomedical imaging. The X-ray image is converted directly into an electrical signal in the photoconductive layer without image blurring. In synchrotron radiation radiography, a long source-to-object distance and a small source spot can produce high-resolution images. Microangiographic images were obtained without image blurring and were stored in a digital frame memory system with a 1024 × 1024-pixel, 10-bit format. In imaging experiments, vasoconstriction and vasodilatation of small cerebral arteries were visualized in response to hypercapnia, hemorrhagic hypotension, and vasoactive agents after iodine contrast agent injection into the carotid artery.

I. INTRODUCTION

MEDICAL imaging using synchrotron radiation has been investigated since intravenous coronary angiography research was begun at the end of 1970s. This safe intravenous angiography technique is useful in place of conventional selective coronary arteriography. Research groups in several synchrotron radiation facilities have improved imaging systems for human studies [1–6]. In addition to intravenous coronary angiography, an intra-arterial microangiography system was developed at the Photon Factory for laboratory animal studies to obtain high-resolution images of small blood vessels: the penetrating transmural coronary arteries [7] and vasodilatation of the arterial circle of cerebrum and its branches [8] in dogs, collateral microvessels following therapeutic angiogenesis in rats [9], and tumor-derived angiogenic vessels in mice [10].

In place of synchrotron radiation, an X-ray generator with a small focal spot has been employed for microangiography using an X-ray direct-conversion type VIDICON camera as a two-dimensional high-resolution detector [11,12]. However, the X-ray generator system has limited capability for

displaying images of blood vessels smaller than 50-μm diameter: images cannot be magnified without focal-spot blurring. Furthermore, a conventional diagnostic angiography system incorporating an X-ray image intensifier and a video camera is not intended for detection of vessels smaller than 200 μm diameter because it is designed for large-field digital angiographic imaging with a 1024 × 1024-pixel format [7].

At SPring-8, a digital microangiography system with spatial resolution as high as 6 μm was developed using an X-ray direct-conversion type detector incorporating an X-ray SATICON pickup tube for depiction of tumor-derived angiogenic vessels in a rabbit model of cancer [13]. The imaging system was also applied to clarify the basal tone and microvascular reactivity in endothelial NO synthase (eNOS)-overexpressing transgenic mice [14].

For this study, we performed cerebral microangiography in rats and mice and particularly undertook radiographical evaluation of changes in small arteries that had not been observed previously. Small arteries branching directly from major trunk vessels, known as perforators, supply arterial blood to the basal nucleus. These perforators are important arteries when considering the effects of systemic disease on cerebral vessels. Vasoconstriction and vasodilatation of the small cerebral arteries were visualized in response to hypercapnia, hemorrhagic hypotension, and vasoactive agents after injection of iodine contrast agent into the carotid artery [15,16].

II. IMAGING SYSTEM

A. Synchrotron Radiation

A useful source of synchrotron radiation is a storage ring, which maintains an electron beam at relativistic speeds in a closed trajectory for many hours using bending magnets. By bending the path of electrons at relativistic speeds, X-rays are emitted at each bending magnet in a direction tangential to beam trajectory. Fig. 1 shows an experimental arrangement at the SPring-8 BL28B2 beamline for X-ray imaging using monochromatic synchrotron radiation X-rays. Microangiographic imaging for depiction of tumor-derived angiogenic vessels in rabbits [13] and microvascular reactivity in transgenic mice [14] were performed at the BL20B2 beamline. Cerebral microangiographic imaging, however, was carried out at the BL28B2 because this beamline, employing a single crystal monochromator,

produces higher-flux X-rays than those at the BL20B2, which uses a double-crystal monochromator.
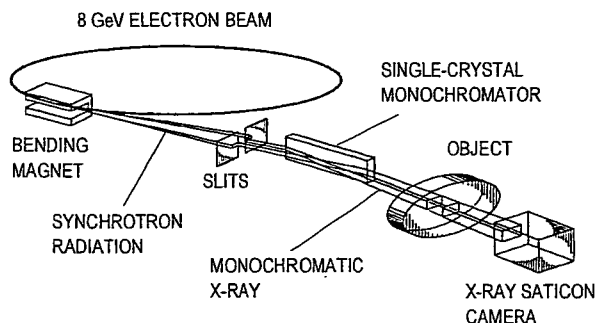

Fig. 1. An illustration of an experimental arrangement for synchrotron radiation microangiography.

Synchrotron radiation generated by bending magnets produces a fan-shaped beam and has a broad and continuous spectrum from infrared to the X-ray region. The single crystal monochromator selects a single energy of synchrotron radiation. Consequently, X-rays with a small energy bandwidth are used for imaging. A rotating-disk X-ray shutter, which is situated between the monochromator and the object, produces pulsed monochromatic X-rays (Fig. 1). The shutter consists of two disks with radial slots rotating about an axis parallel to the X-ray beam. The radial slot width can be changed to adjust the duration of X-ray pulses according to the rotation of one disk with another one. A large amount of disk metal is used to block the beam, resulting in considerably higher attenuation of X-rays, while maintaining low inertia in the disks. The disks rotate to match timing with synchronous signals of a video camera.

Pulsed monochromatic X-rays transmitted through the object are detected using the X-ray direct-conversion type detector, which incorporates the X-ray SATICON pickup tube. The distance between the point-source in the bending magnet and the detector was about 46 m. A nearly parallel X-ray beam was used for imaging without image blur because of the small size X-ray source and the extremely long source-to-object distance. The storage ring was operated at 8 GeV electron beam energy and the beam current was 100 mA. Monochromatic X-ray energy was adjusted to 33.2 keV, which was slightly above the iodine K-edge energy to produce the highest contrast image of the iodine contrast agent. X-ray flux at the object position was ca. 1×10^{10} photons/mm^2/s in imaging experiments.

B. Real-Time Detector

The camera system shown in Fig. 2 comprises a camera head incorporating the X-ray SATICON pickup tube and a camera control unit with an analog-to-digital converter for digital signal output. X-rays enter the SATICON tube through an aluminum window. Fig. 3 shows that absorbed X-rays in

the photoconductive layer are converted directly into electron-hole pairs. Charge carriers generated by X-rays are transported across the photoconductive layer by an electric field. Then, a charge-density pattern is formed on the photoconductive layer surface. The electrostatic image on the surface is read out by a scanning beam of low-velocity electrons to produce a video signal. In Fig. 3, X-ray absorption depends on the photoconductive layer thickness. Thickness of amorphous selenium is 25 μm, yielding a detection efficiency of 14.2% for 33.2 keV X-rays.
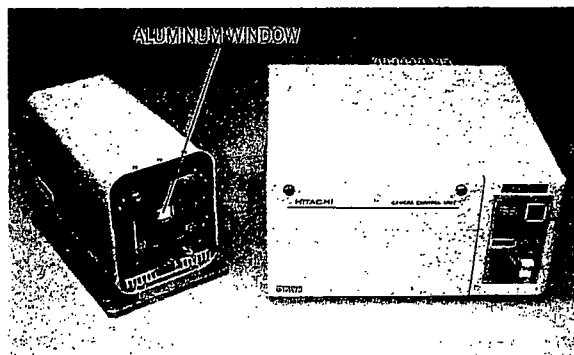

Fig. 2. Photograph of the X-ray SATICON camera system consisting of a camera head (left) and a camera control unit (right).
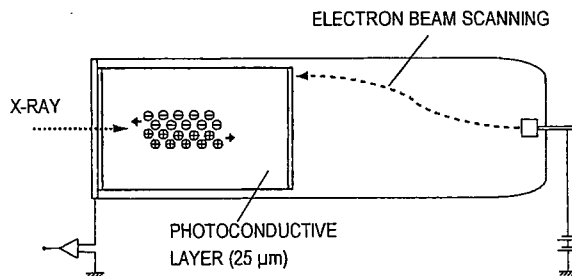

Fig. 3. Schematic cross-section of the SATICON tube. The tube is a glass cylinder maintained under vacuum; the front end of the tube is a flat plate with a diameter of 1 inch, the inside of which is coated with a 25-μm photoconductive material.

In a normal imaging mode with the detector's input field of view of 9.5 mm × 9.5 mm, an equivalent pixel size is 9.5 μm in the case of a 1024 × 1024-pixel format. On the other hand, in zoom imaging modes, the input fields are, respectively, 7.0 mm × 7.0 mm and 4.5 mm × 4.5 mm with pixel size of 7.0 and 4.5 μm. The camera can take sequential images at a maximum speed of 30 images per second. Then the image signals are converted to digital data with the 1024 × 1024-pixel and 10-bit format using an analog-to-digital converter installed in the camera control unit shown in Fig. 2. Digital images are stored in 2 GB RAM of a custom-designed frame memory system after analog-to-digital conversion. Image storage is synchronized with electron-beam scanning

in the pickup tube. A personal computer system controls the entire imaging system, including the camera control unit and the frame memory system.

C. Microangiography

Performance of the direct-conversion type detector was evaluated by taking images of a custom-designed gold resolution chart. The chart thickness was 5 μm; the bar pattern widths were 5.0–12.1 μm. After that, male 6-month-old rats weighing 450–600 g and male 10–12-week-old mice weighing 26–29 g were used for microangiographic imaging experiments.

The animals were anesthetized using sodium pentobarbital intraperitoneally. The right external carotid artery was cannulated in the retrograde direction, with the top of the cannula placed close to the common carotid artery so that all the injected contrast agent went into the common carotid artery without affecting the normal blood flow in the internal carotid artery. The rats and mice were held rigidly on a frame with a specially shaped head holder and ear bars. The frame was then fixed vertically to the X-ray beam to obtain axial views of the cerebral arteries.

All animal experiments conformed to the SPring-8 Guide for Care and Use of Laboratory Animals, and all animal experiments were conducted according to the guidelines for animal experiments at Kobe University Graduate School of Medicine.
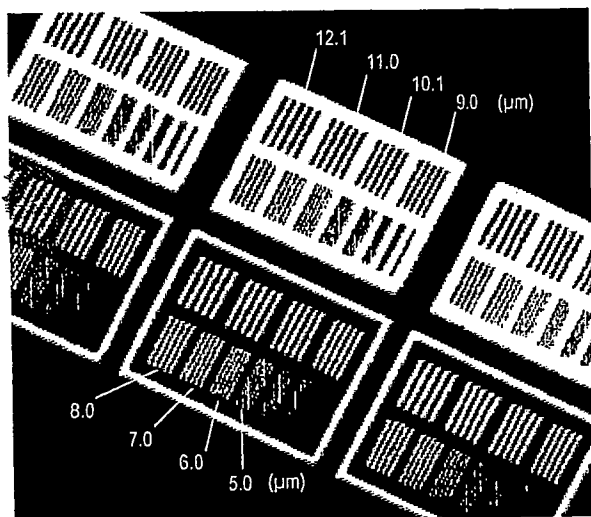
energy of 20.0 keV. Fig. 4 shows an image of the 5-μm-thick chart; the 6.0-μm-wide bars are visible. The limiting spatial resolution is about 6.0 μm in the zoom imaging mode. The 6.0 μm bar width is comparable to the capillary blood vessels' size. Images of the capillaries are obtainable at an X-ray energy of 33.2 keV just above the iodine K-edge energy to produce the highest contrast image of the iodine contrast agent if capillaries are opacified using a high-density contrast agent. However, the contrast agent is diluted substantially in the blood flow.
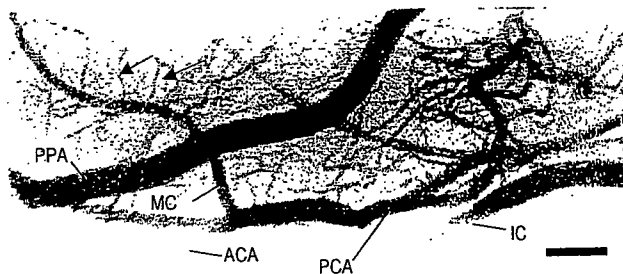

Fig. 5. Synchrotron radiation angiography of a rat showing the anatomy of the cerebral arteries in the brain hemisphere. Black arrows indicate perforating arteries; MCA, middle cerebral artery; ICA, internal carotid artery; ACA, anterior cerebral artery; PCA, posterior cerebral artery; PPA, pterygopalatine artery. Selective imaging was performed in the ICA territory. The scale bar shows 1 mm.

Angiography was performed selectively in the internal carotid artery (ICA) territory. A representative image of the rat cerebral arteries in Fig. 5 was obtained in the normal imaging mode of the detector with the 9.5 mm × 9.5 mm field of view. The smallest detectable vessels were branches of the middle cerebral artery (MCA), which were ca. 30-μm diameter. We confirmed the right ICA, the anterior cerebral artery (ACA), the posterior cerebral artery (PCA), and the pterygopalatine artery (PPA) entirely. We specifically examined the large perforators, which were mostly found arising from the middle cerebral artery trunk. Vasoconstriction and vasodilatation of the large perforators were visualized in response to hypercapnia, hemorrhagic hypotension, and vasoactive agents after iodine contrast agent injection into the carotid artery [15,16].

Fig. 5 depicts a summation result image of 10 consecutive frames in the microangiographic sequence. Original frames, however, were obtained at a rate of 30 frames per second. Image summation was necessary to increase the signal-to-noise ratio and to detect small blood vessels. Furthermore, a temporal subtraction operation was performed for flat-field correction using summation results of 10 consecutive frames acquired before contrast-agent injection. The summation image taken before injection was subtracted from raw images taken after injection to eliminate the superimposed background structure.

Fig. 4. X-ray image of the central area of the 5-μm-thick chart. Numerical values show bar widths. The limiting spatial resolution is around 6.0 μm.

III. RESULTS AND DISCUSSION

An X-ray image of the chart with micrometer-scale bar patterns was obtained in the zoom-imaging mode of the detector with the 4.5 mm × 4.5 mm field of view at an X-ray

3928

We developed a novel cerebral angiography procedure for rats and mice using monochromatic synchrotron radiation X-rays and obtained images of the cerebral perforating arteries for the first time. These results demonstrate the importance of hemodynamic studies in deep brain vessels that had previously been unattainable.

ACKNOWLEDGMENTS

REFERENCES

[1]   E. Rubenstein, R. Hofstadter, H. D. Zeman, A. C. Thompson, J. N. Otis, G. S. Brown, J. C. Giacomini, H. J. Gordon, R. S. Kernoff, D. C. Harrison, and W. Thomlinson, "Transvenous Coronary Angiography in Human Using Synchrotron Radiation," *Proc. Natl. Acad. Sci. U.S.A.*, vol. 83, pp. 9724-9728, 1987.

[2]   W. Thomlinson, "Transvenous Coronary Angiography in Humans," in *Proc. the International School of Physics Enrico Fermi Course CXXVIII, Biomedical Applications of Synchrotron Radiation*, E. Burattini and A. Balerna, Eds. Amsterdam : IOS Press, 1996, pp. 127-153.

[3]   W.-R. Dix, W. Graeff, J. Heuer, K. Engelke, H. Jabs, W. Kupper, and K. H. Stellmaschek, "NIKOS II–A System for Noninvasive Coronary Angiography with Synchrotron Radiation," *Rev. Sci. Instrum.*, vol. 60, p. 2260, 1989.

[4]   T. Dill, W.-R. Dix, C. W. Hamm, M. Jung, W. Kupper, M. Lohmann, B. Reime, and R. Ventura, "Intravenous Coronary Angiography: Experience in 276 Patients," *Synchrotron Radiation News*, vol. 11(2), pp. 12-20, 1998.

[5]   S. Ohtsuka, Y. Sugishita, T. Takeda, Y. Itai, K. Hyodo, and M. Ando, "Dynamic Intravenous Coronary Arteriography Using Synchrotron Radiation and Its Application to the Measurement of Coronary Blood Flow," *Jpn. Circ. J.*, vol. 61(5), pp. 432-440, 1997.

[6]   H. Elleaume, S. Fiedler, F. Estève, A. M. Charvet, B. Bertrand, P. Berkvens, G. Berruyer, F. Brochard, G. Le Duc, C. Nemoz, M. Renier, P. Suortti, W. Thomlinson, and J. F. Le Bas, "First Human Transvenous Coronary Angiography at the European Synchrotron Radiation Facility," *Phys. Med. Biol.*, vol. 45, pp. L39-L43, 2000.

[7]   H. Mori, K. Hyodo, E. Tanaka, M. Uddin-Mohammed, A. Yamakawa, Y. Shinozaki, H. Nakazawa, Y. Tanaka, T. Sekka, Y. Iwata, S. Handa, K. Umetani, H. Ueki, T. Yokoyama, K. Tanioka, M. Kubota, H. Hosaka, N. Ishikawa, and M. Ando, "Small-Vessel Radiography In Situ with Monochromatic Synchrotron Radiation," *Radiology*, vol. 201, pp. 173-177, 1996.

[8]   E. Tanaka, A. Tanaka, T. Sekka, Y. Shinozaki, K. Hyodo, K. Umetani, and H. Mori, "Digitized Cerebral Synchrotron Radiation Angiography: Quantitative Evaluation of the Canine Circle of Willis and its Large and Small Branches," *Am. J. Neuroradiol.*, vol. 20, pp. 801-806, 1999.

[9]   S. Takeshita, T. Isshiki, H. Mori, E. Tanaka, K. Eto, Y. Miyazawa, A. Tanaka, Y. Shinozaki, K. Hyodo, M. Ando, M. Kubota, K. Tanioka, K. Umetani, M. Ochiai, T. Sato, and H. Miyashita, "Use of Synchrotron Radiation Microangiography to Assess Development of Small Collateral Arteries in a Rat Model of Hindlimb Ischemia," *Circulation*, vol. 95, pp. 805-808, 1997.

[10] T. Sekka, S. A. Volchikhina, A. Tanaka, M. Hasegawa, Y. Tanaka, Y. Ohtani, T. Tajima, H. Makuuchi, E. Tanaka, Y. Iwata, S. Sato, K. Hyodo, M. Ando, K. Umetani, M. Kubota, K. Tanioka, and H. Mori, "Visualization, Quantification and Therapeutic Evaluation of Angiogenic Vessels in Cancer by Synchrotron Microangiography," *J. Synchrotron Rad.*, vol. 7, pp. 361-367, 2000.

[11] K. Sada, M. Shirai, and I. Ninomiya, "X-ray TV System for Measuring Microcirculation in Small Pulmonary Vessels," *J. Appl. Physiol.*, vol. 59, pp. 1013-1018, 1985.

[12] M. Shirai, S. Ikeda, K.-Y. Min, A. Shimouchi, T. Kawaguchi, and I. Ninomiya, "Segmental Difference in Vasodilatation due to Basal NO Release in In Vivo Cat Pulmonary Vessels," *Respir. Physiol.*, vol. 116, pp. 159-169, 1999.

[13] K. Umetani, T. Yamashita, N. Maehara, R. Tokiya, S. Imai, and Y. Kajihara, "Small-Field Angiographic Imaging of Tumor Blood Vessels in Rabbit Auricle Using X-ray SATICON Camera and Synchrotron Radiation," in *Proc. 25th Annual Int. Conf. of the IEEE Engineering in Medicine and Biology Society*, Cancún, 2003, pp. 978-981.

[14] T. Yamashita, S. Kawashima, M. Ozaki, M. Namiki, M. Shinohara, N. Inoue, K. Hirata, K. Umetani, and M. Yokoyama, "In Vivo Angiographic Detection of Vascular Lesions in Apolipoprotein E-knockout Mice Using a Aynchrotron Radiation Microangiography System," *Circ J.*, vol. 66, pp. 1057–1059. 2002.

[15] K. Kidoguchi, M. Tamaki, T. Mizobe, J. Koyama, T. Kondoh, E. Kohmura, T. Sakurai, K. Yokono, and K. Umetani, "In Vivo X-Ray Angiography in the Mouse Brain Using Synchrotron Radiation," *Stroke*, vol. 37, pp. 1856-1861, 2006.

[16] A. Morishita, T. Kondoh, T. Sakurai, M. Ikeda, A. K. Bhattacharje, S. Nakajima, E. Kohmura, K. Yokono, and K. Umetani, "Quantification of Distension in Rat Cerebral Perforating Arteries," *NeuroReport*, vol. 17, pp. 1549-1553, 2006.

ピオグリタゾンにより認知機能の改善が認められた
アルツハイマー病を合併した高齢者糖尿病の1例

松沢　俊興　　櫻井　孝　　明嵜　太一　　芳野　弘　　高田　俊宏　　横野　浩一

要約：症例は81歳女性．5～6年前から記銘力障害がゆっくりと進行しており，78歳で糖尿病と診断された．高血圧・肥満を認め，HbA1c 8.7%，HOMA-R 5.08であった．ミニメンタルテスト（MMSE）24点，長谷川式簡易知能スケール（HDS-R）21点，記憶，見当識，遂行機能の低下を認め，National Institute of Neurological and Communicative Disorders and Strokes-Alzheimer's Disease and Related Disorders Association（NINCDS-ADRDA）の probable Alzheiemer's disease（AD）と診断された．塩酸メトホルミン，グリメピリド，塩酸ドネペジルにて加療を行ったが，18カ月後にはMMSE 19点，HDS-R 17点まで脳機能は低下した．そこで血糖改善目的にピオグリタゾンを投与追加したところ，5カ月後に血糖管理はHbA1c 7.9%から6.3%，HOMA-R 5.08（初診時）から2.89に是正された．また同時に介護者から認知機能の改善を示唆する情報があり，6カ月後に神経心理検査で改善が認められた（MMSE 24点，HDS-R 21点）．ピオグリタゾンは peroxiosome proliferators-activated receptor γ アゴニストであり，インスリン感受性を改善させるのみならず，抗炎症作用・神経保護作用を有する．本例はADを合併した高齢者糖尿病で，ピオグリタゾン投与により脳機能の改善が認められた1例と考えられた．
Key words：① 高齢者糖尿病　② アルツハイマー病　③ ピオグリタゾン

はじめに

ブドウ糖は脳の主たるエネルギー代謝の基質であり，糖代謝異常は脳機能に影響する．急性高血糖では脳機能は可逆性に低下し，2型糖尿病および耐糖能異常でも認知機能は低下している[1]．最近の疫学調査では，糖尿病は脳血管性認知症のみならずアルツハイマー病（以下ADと略す）の危険因子である可能性が指摘されている[2,3]．なかでも最も信頼性の高いロッテルダム研究では，高齢者糖尿病でのAD発症の相対危険度は1.9倍と有意に高く，インスリン使用者では4.3倍と高値であることが報告された．一方，ADの約80%に2型糖尿病および耐糖能異常がみられるとする報告もある[4]．また糖尿病とADの分子生物学的な関連を示す報告も蓄積されつつあり，糖尿病とADにおける高インスリン血症の関与に関心が集まっている．今回ADを合併した高齢者2型糖尿病で，ピオグリタゾン投与により認知機能の改善を認めた症例を経験したので報告する．

症　例

患者：81歳，女性．

主訴：物忘れ．

既往歴：70歳時から高血圧，抗コリン剤やH₂受容体拮抗薬の内服はなし

家族歴：特記すべきことなし

嗜好：喫煙歴（－），飲酒歴（－）

現病歴：1998年頃から，料理の献立が減る，電話の取り次ぎができない，同じものばかり買ってくることに家族が気づいていた．77歳時に頭部MRI検査を受けたが異常所見は指摘されなかった．夫の死亡を契機に抑うつ傾向となり，抗うつ薬の投与を受けていた．78歳にて近医で糖尿病と診断され，食事・運動療法を始めた．その後も同じことをくり返し話す，家族との約束を忘れるなどの記銘力障害が進行し，血糖

Table 1　Laboratory data on admission

Urinalysis		Blood chemistry		Fasting IRI	$14\,\mu$U/ml
Glucose	(−)	TP	6.2 g/dl	HOMA-R	5.08
Protein	(−)	Alb	3.6 g/dl	TSH	$5.884\,\mu$U/ml
Ketone	(−)	T-bil	0.4 mg/dl	FT$_3$	2.8 pg/ml
Blood	(−)	AST	27 IU/l	FT$_4$	1.05 ng/dl
Alb	12 mg/gCr	ALT	36 IU/l	Vit. B$_1$	42 ng/ml
		LDH	155 IU/l	Vit. B$_{12}$	402 pg/ml
Peripheral blood		BUN	14 mg/dl	Folic acid	7.0 ng/ml
WBC	6,900 /μl	Cre	0.55 mg/dl		
RBC	331×10^4/μl	Na	141 mEq/l	ApoE phenotype(3, 3)	
Hb	10.0 g/dl	K	3.5 mEq/l		
Ht	30.9%	Cl	107 mEq/l	Cerebrospinal fluid	
PLT	13.9×10^4/μl	TC	206 mg/dl	Appearance : colorless	
		HDL-cho	40 mg/dl	The initial pressure : 140 mmH$_2$O	
Serology		TG	168 mg/dl	Cell : 1/mm^3(mononuclear cell)	
CRP	0.2 mg/dl	Glucose	147 mg/dl	TP : 58 mg/dl	
TPHA	(−)	HbA1c	8.7%	Glucose : 110 mg/dl	
FTA-ABS	(−)				
HbsAg	(−)				
HCVAb	(−)				

コントロールも悪化したため，精査加療目的にて当科に入院した．

入院時現症：身長 149 cm，体重 64 kg，BMI 29 kg/m²，意識清明，血圧 144/90 mmHg，脈拍 78 回/分・整，心肺腹部所見に異常を認めない．

眼底検査：異常なし．

神経学的所見：右利き．両側アキレス腱反射は減弱．

神経伝導速度検査：腓腹神経の感覚神経活動電位振幅の低下．

入院時検査成績(Table 1)：血液検査では高血糖(空腹時血糖は 150～170 mg/dl)，高インスリン血症を示す他，特記すべき異常は認めない．髄液検査でも異常はなかった．アポタンパク E フェノタイプは E3/3 であった．

神経心理検査：ミニメンタルテスト (Mini mental state examination；以下 MMSE と略す)24 点，長谷川式簡易知能スケール(Hasegawa dementia scale-revised；以下 HDS-R と略す)21 点と境界域であり，時間，場所見当識，注意・計算，物品再生，視覚的短期記憶，言語の流暢性が減点項目であった．武蔵病院記憶テスト[5]では，言語性・視覚性記憶，特に遅延再生の強い低下，注意力障害を認めた．抑うつ傾向は認めなかった．さらに実行機能障害が認められ，National Institute of Neurological and Communicative Disorders and Strokes-Alzheimer's Disease and Related Disorders Association (以下 NINCDS-ADRDA と略

す)の probable AD と診断された[6]．

頭部画像検査(Fig. 1)：MRI では，左優位の側頭葉と側頭葉内側に軽度の脳萎縮を認めた．脳血流シンチにて両側の頭頂葉と左優位に側頭葉の血流低下を認めた．

脳波：基礎波 10 Hz，振幅 60～80 μV，α 波は後頭葉優位でやや不規則で量は中等量，Waxing や waning 無し，開眼抑制は完全，突発波なし，徐波なく，正常脳波であった．

臨床経過(Fig. 2)：糖尿病に対してインスリンの分泌作用を増強するスルホニルウレア薬であるグリメピリド(1 mg/day)，インスリン作用，もしくはインスリン感受性を増強するビグアナイド剤である塩酸メトホルミン(500 mg/day)を投与し，6 カ月後には HbA1c 7.3%，空腹時血糖 110～140 mg/dl 程度に血糖コントロールは改善された．しかし再び糖尿病コントロールは悪化し，18 カ月後には HbA1c 7.9%，空腹時血糖 130～160 mg/dl 程度に増悪した．AD に対して塩酸ドネペジルの投与を行っていたが，18 カ月後には MMSE 19 点，HDS-R 17 点までの悪化を認めた．そこで血糖コントロール目的のためインスリン感受性を改善させる，ピオグリタゾン(15 mg/day)を追加投与したところ，5 カ月後には HbA1c 7.9% から 6.3% に，朝食前血糖 80～110 mg/dl，HOMA-R 5.08(初診時)から 2.89 に改善した．また同時に介護者から，日常生活において，自発的に料理をする，味付けが良くなる，電話のメモをとる，積極的に外出する，嫁を名
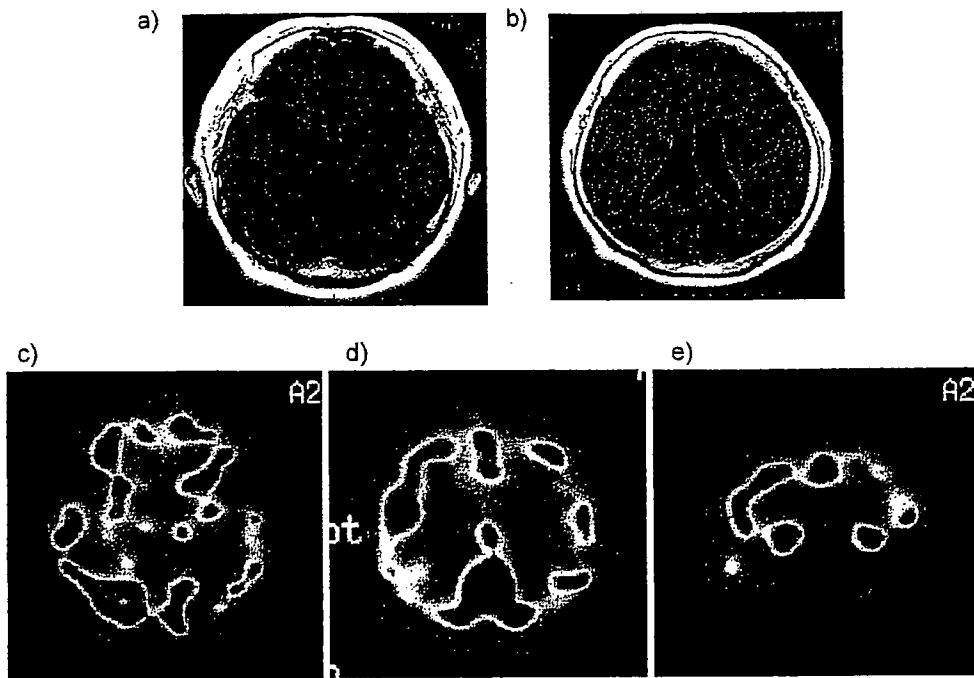
a) b)

c) d) e)

Fig. 1 Brain MRI · SPECT

a : T1-weighted MRI, mid-brain level. Lt. dominant medial temporal cortex atrophy.

b : T1-weighted MRI, parietal lobe level.

c, e : IMP SPECT. Decreased blood flow in lt. dominant temporal lobe.

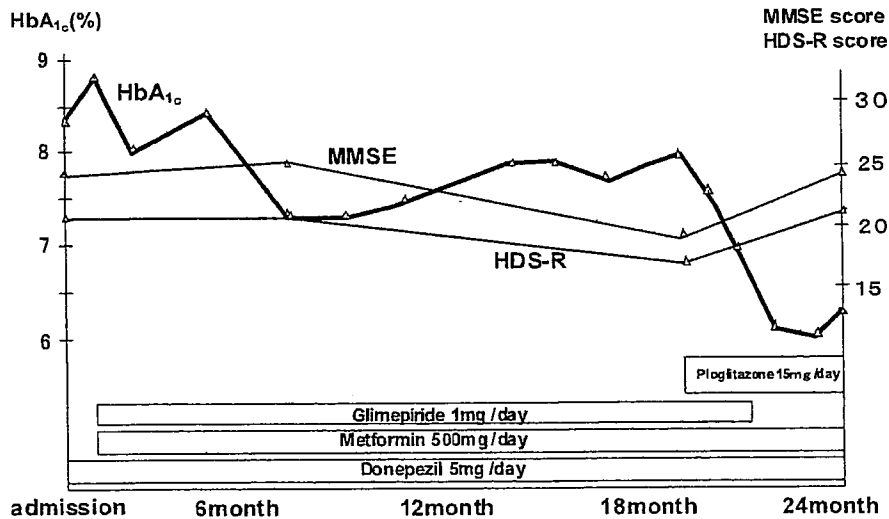d : IMP SPECT. Decreased blood flow in parietal lobe.

Fig. 2 Clinical course

前で呼ぶ，などの行動改善がみられたとの情報が得ら
れた．ピオグリタゾン投与6カ月後には心理検査で
も，MMSE 24点，HDS-R 21点まで改善した（遅延再
生，見当識の改善）．頭部MRI，脳血流シンチ，脳波
の所見には変化はみられなかった．

考　察

本例は，肥満・高血圧を伴う2型糖尿病にADが

合併した高齢者である．強い遅延再生の低下，時間見
当識，注意力の低下，実行機能障害が認められAD
と診断された．脳画像検査もADの特徴を示してい
た．高インスリン血症改善を念頭においた糖尿病の管
理，塩酸ドネペジルによるAD治療が行われたが，
治療開始後18カ月には認知障害は悪化した．ここで
ピオグリタゾンが投与され，高血糖・高インスリン血
症の急速な是正（HOMA指数は初診時の2004年3月